Chapter 8

Failure Model

8.1 General

Although the formulations presented so far attempt to explain the load-slip relation of a multiple-bolt joint, the model is still incomplete since no consideration is given as to whether material strength might be exceeded at certain displacement levels. This is especially important in a multiple-bolt joint, for changes in fastener spacing and number of fasteners may induce stress concentrations causing catastrophic failure.

Without the reliance on fracture mechanics, the failure model presented here employs a novel method to predict brittle failure within the joint. Quintessentially, failure stresses are predicted based on interface friction between bolt and wood, and material deformation of the members attributable to the bolt. The formulation applies to both rigid and slender bolts. Unlike the closely tied modified hysteresis and structural models, the failure model is a separate, stand-alone entity whose only input is displacement and local member stiffness from which material strength is derived. Thus, it can be easily integrated into other models such as uni-directional models. Model output controls forces computed by the modified hysteresis / structural model. If failure is detected, forces are effectively reduced.

8.2 Displaced Volume Method

A new method named the "Displaced Volume Method" (DVM) is derived here that is ultimately used to compute stresses around slender and rigid bolts. DVM evades the difficulty of computing stresses in orthotropic materials for cases where the plane stress assumption is not valid such as slender bolts. The great advantage of DVM is that it allows the relative simple closed-form computation of local forces for both slender and rigid bolts. Once forces are identified, stress distributions can be computed (Sec. 8.3) and a failure criterion applied (Sec. 8.4). Based on the Yield Theory, Jorissen's crack model (Jorissen 1998), and a mechanics approach, DVM is a robust method whose equations are comparatively easily programmed. In combination with stress computations and appropriate failure criteria, failure is predicted as a function of important parameters such as fastener spacing and end distance, fastener diameter, yield mode, member thickness, member width, and general material properties.

The idea behind DVM is similar to a buoyancy problem. If it is assumed that the wood foundation is a collection of individual, independent linear springs, then the reactive force exerted by the foundation on a body that is pushed into it is proportional to the displaced volume. The proportionality factor is the three-dimensional foundation modulus. The fact that the wood foundation is modeled by linear springs, despite the well established notion that that wood generally exhibits non-linear behavior, is no limitation since only failure is of interest. Catastrophic failure is described by a single point on the load-slip curve of the joint. How that point is reached, whether by linear or non-linear behavior is immaterial in this case.

If the foundation can be visualized as an array of an infinite number of independent linear springs, and if it is assumed that the dowel is infinitely stiff along its length, then the reaction force of a dowel with diameter *d*, plotted in three-dimensional space as a function of length (*z*-direction), deformation (*x*-direction), dowel diameter, and reaction per unit length (*p*-direction) resembles a triangular plane as depicted in Figure 8.1. The net force necessary to rotate the dowel about the point predicted by the Yield Theory is equal to the more darkly shaded area. However, the total force on the dowel equals the area of all triangular planes along its length. Observe that all forces act in the *x*-*z*-plane parallel to the x-axis.

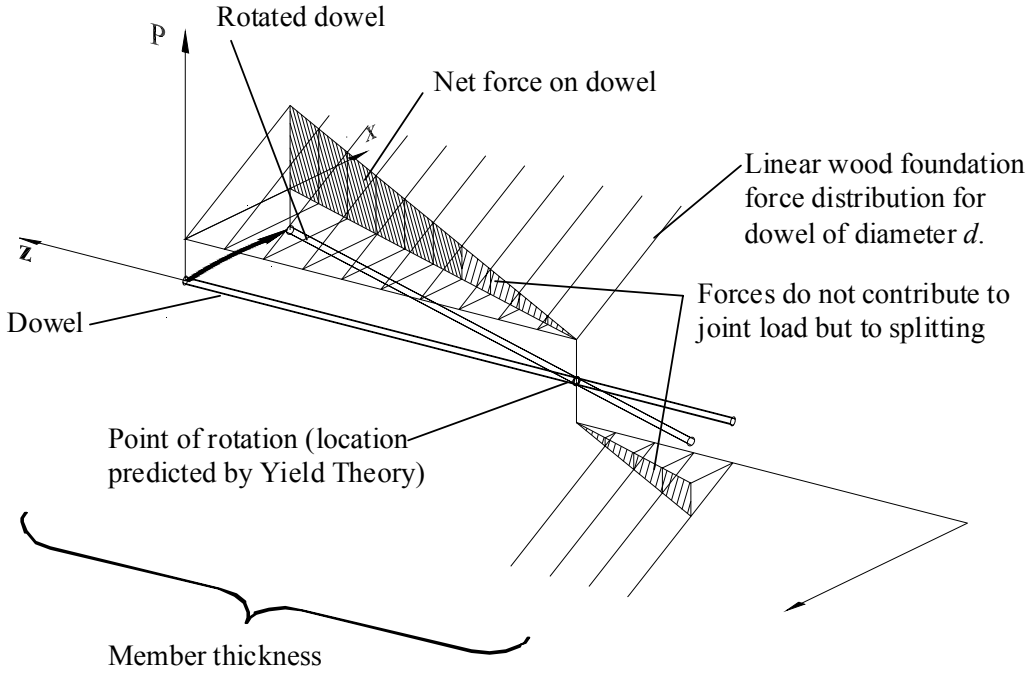

Figure 8.1: Reaction force (shaded area) determined by the displaced volume of the dowel assuming that the foundation can be modeled as an array of linear, independent springs.

As the joint is displaced, the bolt rotates and ultimately deforms similar to one of the modes described by the Yield Theory. For example, rotating in accordance to Mode II, the bolt displaces volume as it is pressed into the wood foundation as depicted in Figure 8.2. If the foundation modulus is known, total reaction force of the foundation can be computed and from it shear stresses and stresses perpendicular to the grain are obtained.

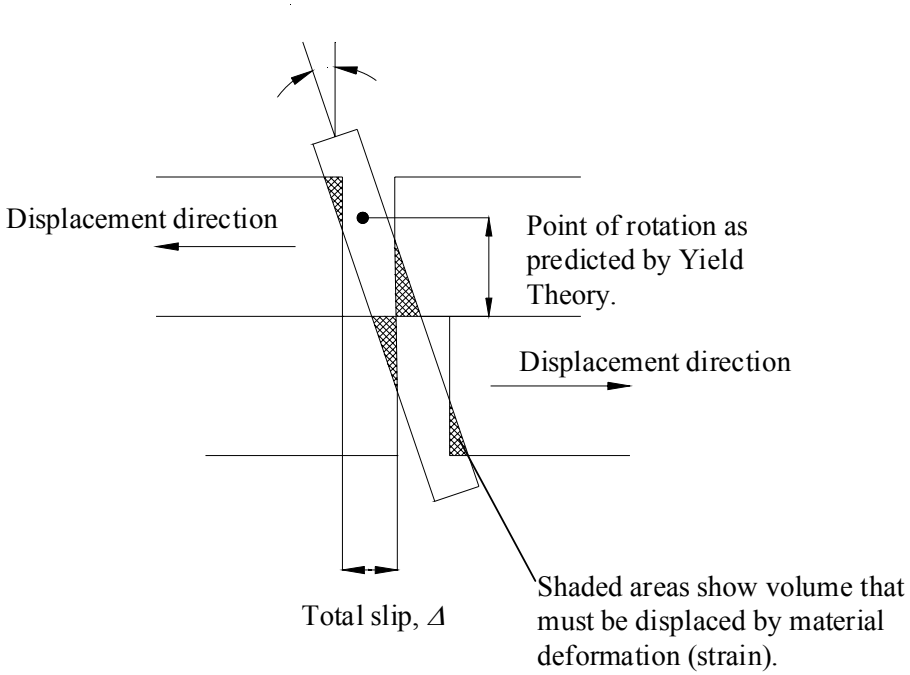

Figure 8.2: Displaced volume shown on a bolt deforming in Mode II

8.2.1 Crack Formation and Stresses Perpendicular to the Grain

In a multiple-bolt joint, failure typically occurs due to a combination of perpendicular to grain stresses and shear stresses. Observations from experiments confirm that joint failure can be most frequently classified as plug shear or splitting.

If a cylindrical body like a bolt is pressed into a wood foundation (real foundation, not approximated by independent springs), stresses perpendicular to the grain develop attributed to the resultants of the reaction forces on the surface of the dowel. Furthermore, recall from Chapter 2 that, depending on the angle of friction, some fibers are deviated around the bolt, whereas others are crushed underneath it, ultimately leading to the formation of two cracks as the bolt gets pushed farther into the foundation. According to Jorissen (1998), the width of the compression region parallel to the grain may be determined by

$$\delta = 2 \cdot r_{bolt} \cdot \sin(\varphi) = d_{bolt} \cdot \sin(\varphi) \tag{8.1}$$

		Units[1]
d_{bolt}	fastener diameter	mm
φ	angle of friction	
δ	width of compression region	mm

In other words, as a result of friction between the bolt–wood interface, one may assume that there are pronounced "regions" where the foundation is stressed parallel and perpendicular to the grain, respectively (Figure 8.3). If this is true, then acting shear stresses can be computed based on the volume displaced within the compression region parallel to the grain. On the other hand, stresses perpendicular to the grain can be determined in relation to the volume displaced within the compression region perpendicular to the grain.

[1] All units in this chapter are specified as used in MULTBOLT.

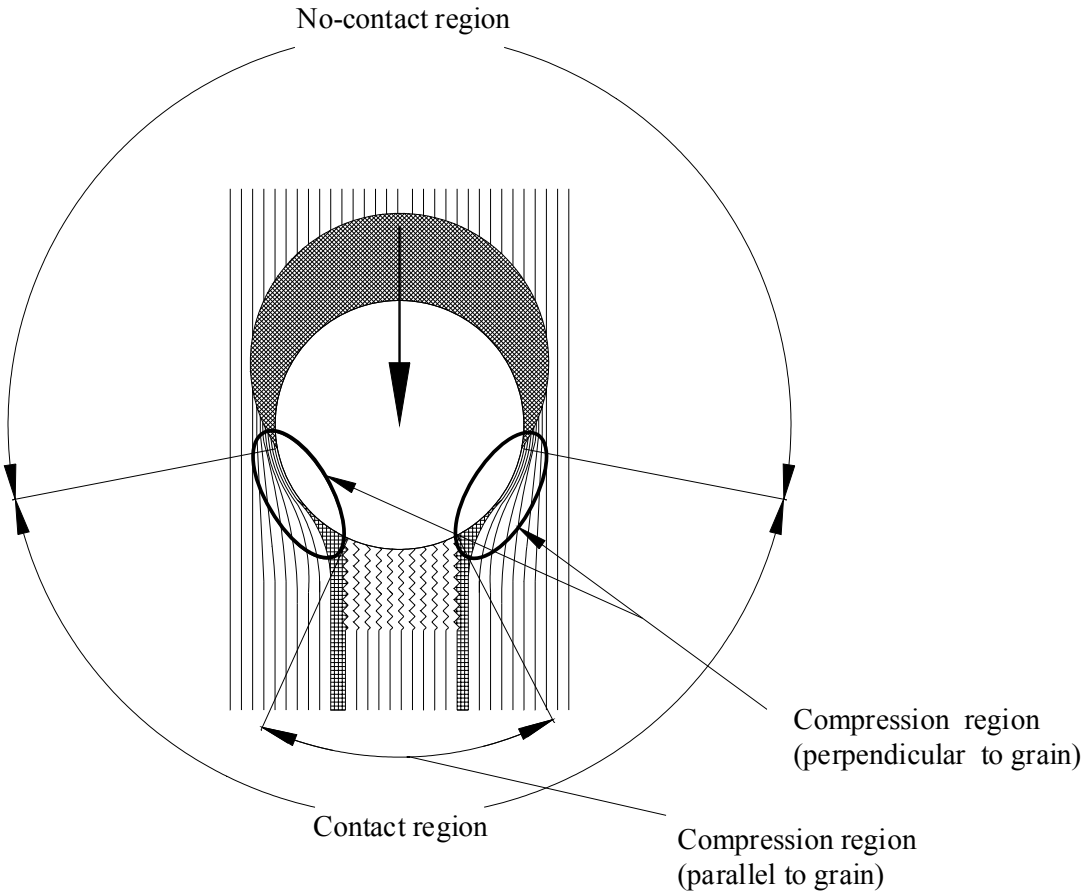

Figure 8.3: Attributed to friction, the contact region may be divided into regions where stresses parallel to the grain dominate and a region where stresses perpendicular to the grain dominate.

8.2.2 Computation of Displaced Volume

Displaced volumes are directly related to their cross-sectional areas, which are derived first. Slack and differences in slack between directions of movement are included in all derivations although the exact location of the bolt within the hole is not known (refer to Section 5.5). What is known, however, is total slack in positive ($slack_p$) and negative ($slack_n$) direction of movement. Since for most practical purposes oversize << bolt diameter, it is assumed that the bolt is located such that

$$slack_p, Member1 = slack_p, Member2 \tag{8.2}$$

and

$$slack_n, Member1 = slack_n, Member2 \tag{8.3}$$

It is further assumed that slack does not affect the point of rotation as predicted by the Yield Theory. Both area and volume output were verified by the graphical program AutoCAD R14 (1999).

8.2.2.1 Strain Areas Parallel and Perpendicular to the Grain

In plane view (parallel to the shear plane of the joint), a round bolt pushing into the wood foundation of an oversized hole may be abstracted as two intersecting circles with different diameters as depicted in Figure 8.4. Observe that this aids to simplify the analysis. Actual cross section of the rotated bolt in plane view is an ellipse. The formulation is later adjusted to yield more accurate results.

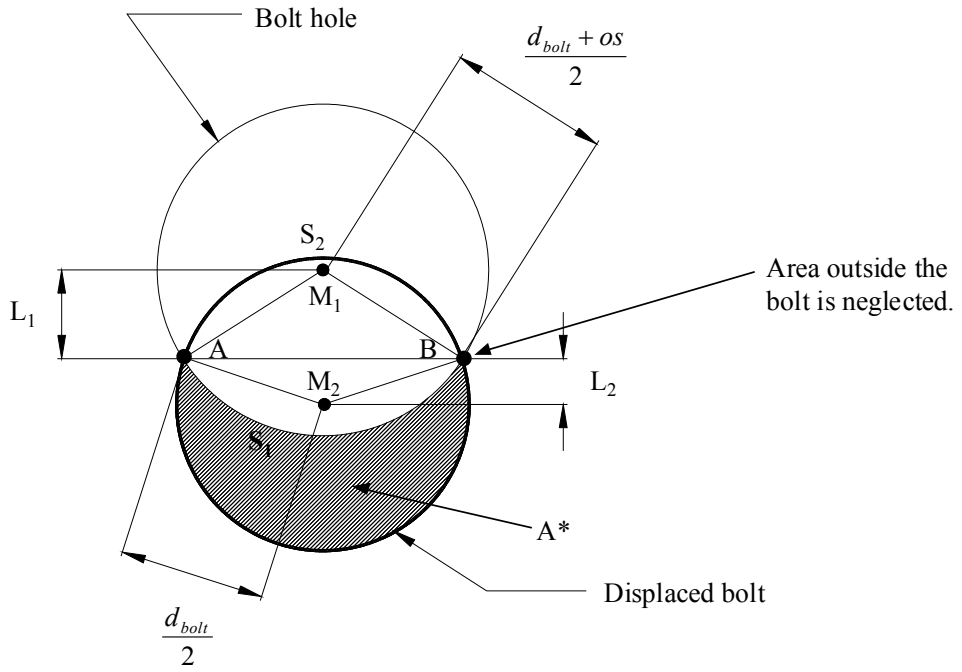

Figure 8.4: Crescent area, *A**, of two intersecting circles with different diameters. *os* is total oversize and *S* denotes the length of the arc under consideration.

Considering Figure 8.4, let

$$\Delta = L_1 + L_2 \tag{8.4}$$

The goal is to relate mathematically the crescent area A* to the displacement Δ. Given that

$$R_1 = \frac{d_{bolt} + os}{2} \tag{8.5}$$

$$R_2 = \frac{d_{bolt}}{2} \tag{8.6}$$

$$A_{bolt} = \pi \cdot R_2^2 \tag{8.7}$$

by making use of the Pythagorean Theorem, it follows

$$R_1^2 - L_1^2 = R_2^2 - L_2^2 \tag{8.8}$$

Solving Equation (8.4) for L_2 and substituting the result into Equation (8.5) yields

$$L_1^2 = -R_2^2 + L_2^2 + R_1^2 = -R_2^2 + (\Delta - L_1)^2 + R_1^2$$
$$L_1^2 = -R_2^2 + \Delta^2 - 2L_1\Delta + L_1^2 + R_1^2 \tag{8.9}$$

Reordering Equation (8.9), it can be written

$$L_1 = \frac{R_1^2 - R_2^2 + \Delta^2}{2\Delta} \tag{8.10}$$

and substituting into Equation (8.4) yields

$$L_2 = \Delta - \frac{R_1^2 - R_2^2 + \Delta^2}{2\Delta} \tag{8.11}$$

The segmental area of each circle may be defined as

$$Area[ABS_1] = R_1^2 \cdot \arccos\left(\frac{L_1}{R_1}\right) - L_1\sqrt{R_1^2 - L_1^2} \tag{8.12}$$

$$Area[ABS_2] = R_2^2 \cdot \arccos\left(\frac{L_2}{R_2}\right) - L_2\sqrt{R_2^2 - L_2^2} \tag{8.13}$$

It follows for A^*

$$A^* = A_{bolt} - (Area[ABS_1] + Area[ABS_2]) \tag{8.14}$$

Finally, substitution and simplification yields

$$A^* = \frac{1}{8} \cdot \left[2 \cdot d_{bolt}^2 \cdot \pi + \Delta \cdot \sqrt{-\frac{\left(os^2 - 4 \cdot \Delta^2\right) \cdot \left(4 \cdot d_{bolt}^2 + 4 \cdot d_{bolt} \cdot os + os^2 - 4 \cdot \Delta^2\right)}{\Delta^2}} - 2 \cdot d_{bolt}^2 \cdot \arccos\left(-\frac{2 \cdot d_{bolt} \cdot os + os^2 - 4 \cdot \Delta^2}{4 \cdot d_{bolt} \cdot \Delta}\right) - 2 \cdot (d_{bolt} + os)^2 \cdot \arccos\left(\frac{2 \cdot d_{bolt} \cdot os + os^2 - 4 \cdot \Delta^2}{4 \cdot d_{bolt} \cdot \Delta + 4 \cdot os \cdot \Delta}\right) \right] \tag{8.15}$$

		Units
A^*	Crescent area of intersecting circles	mm^2
os	bolt-hole oversize	mm
Δ	total displacement	mm
d_{bolt}	fastener diameter	mm

Attributed to the fact that oversize << bolt diameter, it can be observed from Figure 8.5 that the relationship of A^* and Δ is almost linear except at larger displacements. Yet, a linear relationship for larger displacements is actually closer to reality because the area outside the bolt was neglected in the derivation.

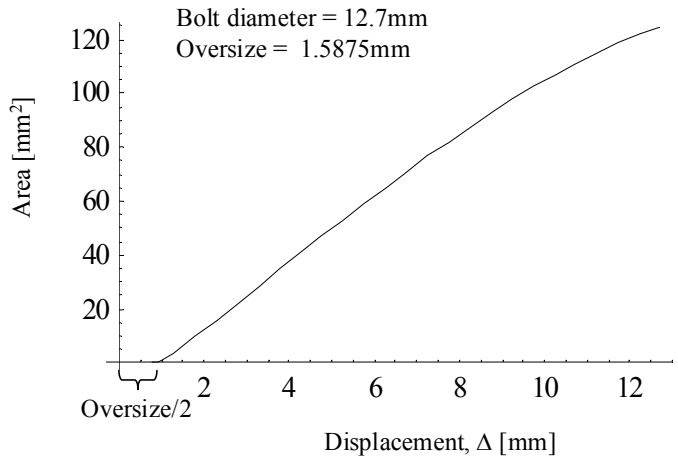

Figure 8.5: Plot of A^* versus Δ.

To obtain the strain area parallel to the grain under consideration that oversize << bolt diameter and using Equation (8.1), it is reasonable to write (Figure 8.6)

$$A_{parallel} \approx d_{bolt} \cdot \sin(\varphi) \cdot \Delta$$

where φ is the angle of friction between bolt and wood foundation.

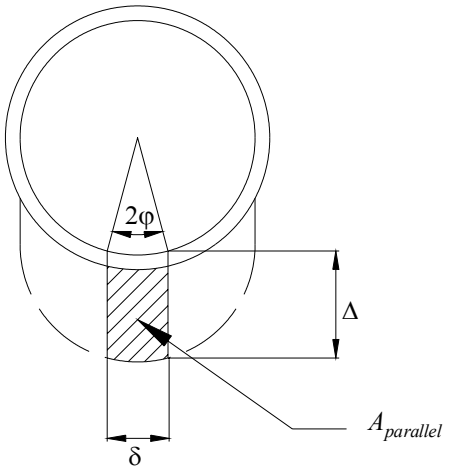

Figure 8.6: Strain area parallel to the grain

It is clear from Figure 8.7 that the strain area perpendicular to the grain is defined as

$$A_{perp} = \frac{A^* - A_{parallel}}{2} \tag{8.16}$$

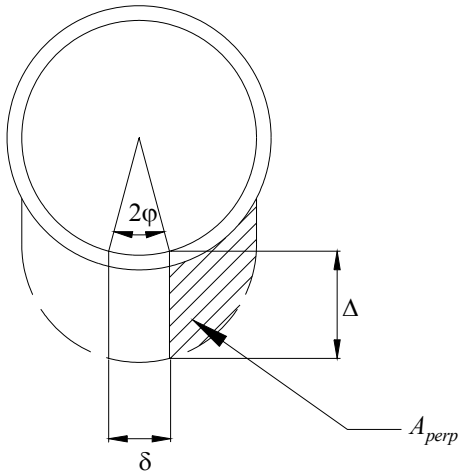

Figure 8.7: Strain area perpendicular to the grain

8.2.2.2 Displaced Volume as a Function of Joint Displacement

8.2.2.2.1 Mode I

The bolt does not rotate when yielding in Mode I, producing a constant strain area along bolt length. MULTBOLT automatically assumes that yielding occurs in the thinner member. This assumption is correct for most cases, but may not be true for some cases with high variation in embedment strength between the members. Recall that the strain areas were derived based on the displacement Δ, which equals the distance between bolt hole center and bolt center. Thus, let

$$\Delta^* = \Delta_{\text{joint}} - \frac{slack_p - slack_n}{2} \quad \text{for } \Delta_{\text{joint}} > 0 \tag{8.17}$$

and

$$\Delta^* = \left|\Delta_{\text{joint}}\right| - \frac{slack_n - slack_p}{2} \quad \text{for } \Delta_{\text{joint}} < 0 \tag{8.18}$$

to account for cases when bolt hole center and bolt center do not coincide at zero displacement. The variables $slack_p$ and $slack_n$ describe the slack in positive and negative direction of movement, respectively. Thus, the displaced volumes for Mode I may be computed as

$$V_{perp} = t_{thin} \cdot A_{perp}(\Delta^*) \tag{8.19}$$

$$V_{para} = t_{thin} \cdot A_{para}(\Delta^*) \tag{8.20}$$

where t_{thin} is the thickness of the thinner member.

8.2.2.2.2 Mode II

Consider the displaced bolt portrayed in Figure 8.8. It is clear that strain area changes along the bolt axis due to rotation. The displaced volume is similar to a crescent wedge. Since it is reasonable to assume that (Figure 8.5)

$$A^* \approx \mathrm{K} \cdot \Delta \tag{8.21}$$

where K is a proportionality factor, the volumes may be defined based on the average strain area, $\overline{A}$, which is obtained at the displacement

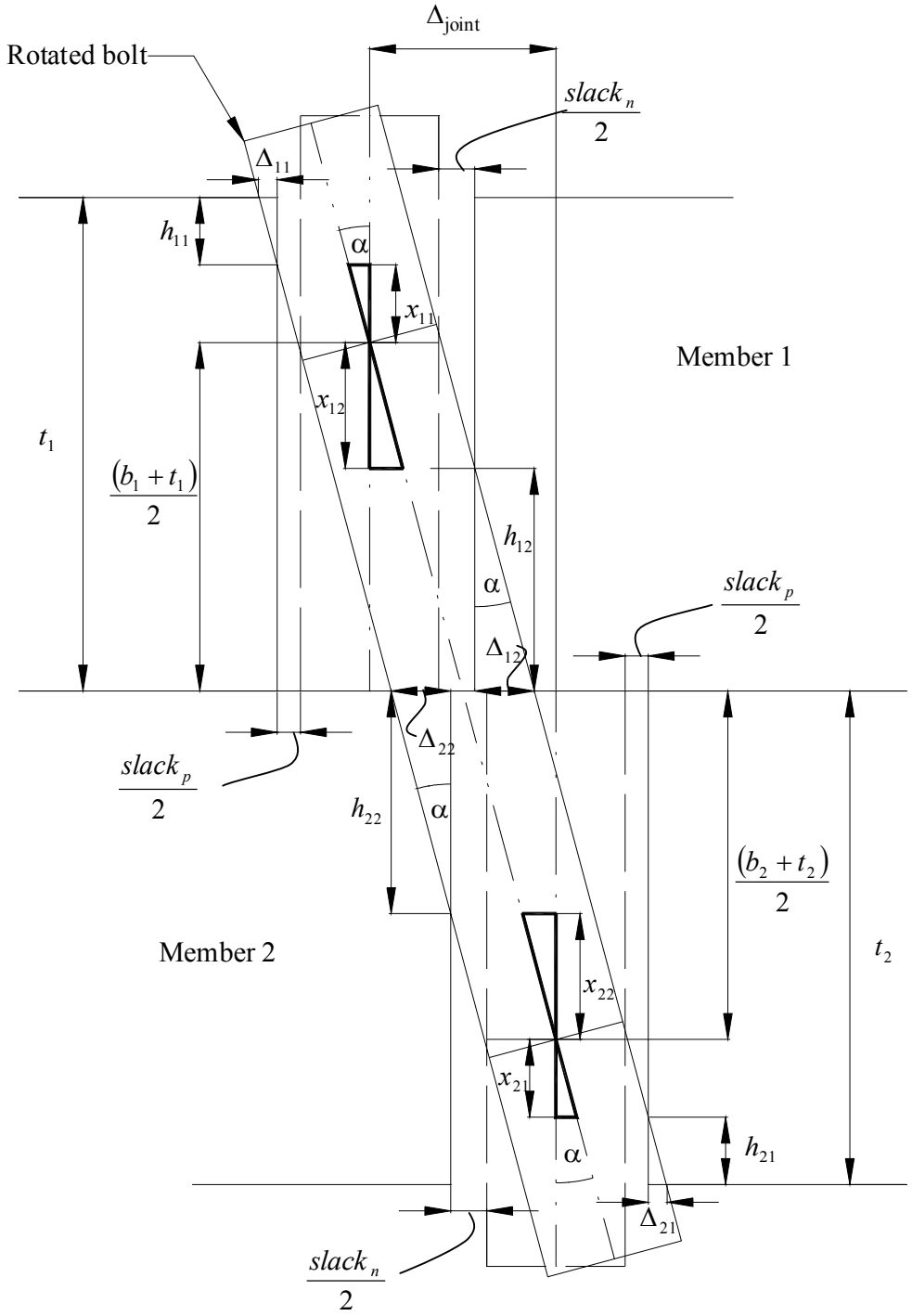

Figure 8.8: Bolt yielding in Mode II. Dimensions shown are used to compute the displaced volumes.

$$\hat{\Delta}_{ik} = \frac{\Delta_{ik}}{2} + \frac{os}{2} \tag{8.22}$$

with

$$i = 1,2 \qquad k = 1,2 \tag{8.23}$$

where *os* = oversize. Thus, a bolt deforming in Mode II displaces the eight volumes (four perpendicular and four parallel)

$$V_{perp,ik} = h_{ik} \cdot \overline{A}_{perp}(\hat{\Delta}_{ik}) \tag{8.24}$$

and

$$V_{para,ik} = h_{ik} \cdot \overline{A}_{para}(\hat{\Delta}_{ik}) \tag{8.25}$$

where *i* and *k* are as before and

$$h_{i1} = \frac{t_i - b_i}{2} - x_{i1} \tag{8.26}$$

$$h_{i2} = \frac{b_i + t_i}{2} - x_{i2}$$

The variable b_i is obtained by the European Yield Theory equations as described in Section 2.1.4.1 (Chapter 2). But x_{ik} is defined as

$$x_{ik} = \frac{sl}{\tan\alpha} \tag{8.27}$$

where, *sl* @ $slack_n/2$ or $slack_p/2$. To relate the displaced volumes to total joint displacement, Δ_{joint}, we can write

$$\tan\alpha = \frac{\left|\Delta_{\text{joint}}\right|}{\frac{b_1 + t_1}{2} + \frac{b_2 + t_2}{2}} \tag{8.28}$$

and

$$\Delta_{ik} = h_{ik} \cdot \tan\alpha \tag{8.29}$$

For Mode II, the lengths b_1 and b_2 are given by the Yield Theory (see Chapter 2 or Hilson 1995)

$$b_1 = \frac{t_1}{1+\beta} \cdot \left(\sqrt{\beta + 2 \cdot \beta^2 \cdot \left(1 + \frac{t_2}{t_1} + \left(\frac{t_2}{t_1} \right)^2 \right) + \beta^3 \cdot \left(\frac{t_2}{t_1} \right)^2} - \beta \cdot \left(1 + \frac{t_2}{t_1} \right) \right) \tag{8.30}$$

$$b_2 = \frac{b_1}{\beta} \tag{8.31}$$

with

$$\beta = \frac{F_{embed1}}{F_{embed2}} \tag{8.32}$$

At this point it is important to revisit the modified hysteresis model and its peculiarities. Because the hysteresis model describes the entire single bolt joint, it smears the different material properties, including embedment strengths, into an average response. Hence, for the purpose of the model developed in this work, the same average embedment strength is used for each member, and therefore

$$b_1 = b_2 \tag{8.33}$$

Thus, Equation (8.30) simplifies to

$$b_1 = \frac{1}{2} \cdot \left(-t_1 - t_2 + \sqrt{3 \cdot t_1^2 + 2 \cdot t_1 \cdot t_2 + 3 \cdot t_2^2} \right) \tag{8.34}$$

However, if the joint exhibits vastly different embedment strengths per member (for instance when different species are used), one can revert to computing b_1 and b_2 for each member. Changes in the model must be made accordingly.

8.2.2.2.3 Mode III

If a Mode III joint is investigated, the program automatically assumes, similar to Mode I, that the main wood yielding occurs in the thinner member and the plastic hinge forms in the thicker member. Attributed to the plastic hinge, only six volumes need to be computed. Assuming, for the sake of demonstration, that the plastic hinge is located in Member 2 as depicted

in Figure 8.9, we may write (if the hinge is located in Member 1 subscripts must be changed correspondingly)

$$V_{perp,ik} = h_{ik} \cdot \overline{A}_{perp}(\hat{\Delta}_{ik}) \tag{8.35}$$

$$V_{para,ik} = h_{ik} \cdot \overline{A}_{para}(\hat{\Delta}_{ik}) \tag{8.36}$$

where

$$i = 1,2 \qquad k = \begin{cases} 1,2 & \text{for } i = 1 \\ 2 & \text{for } i = 2 \end{cases} \tag{8.37}$$

and

$$h_{11} = \frac{t_1 - b_1}{2} - x_{11} \tag{8.38}$$

$$h_{12} = \frac{b_1 + t_1}{2} - x_{12} \tag{8.39}$$

$$h_{22} = b_2 - x_{22} \tag{8.40}$$

x_{ik} and $\hat{\Delta}_{ik}$ are as defined in Equation (8.27) but the tangent of the rotation angle α changes to

$$\tan\alpha = \frac{\left|\Delta_{\text{joint}}\right|}{\frac{b_1 + t_1}{2} + b_2} \tag{8.41}$$

and in combination with Equation (8.33) and the Yield Theory, b_1 may be written as

$$b_1 = \frac{t_1}{3} \cdot \left(-1 + \sqrt{4 + \frac{12 \cdot M_{yield}}{d_{bolt} \cdot \overline{F}_{embed} \cdot t_1^2}} \right) \tag{8.42}$$

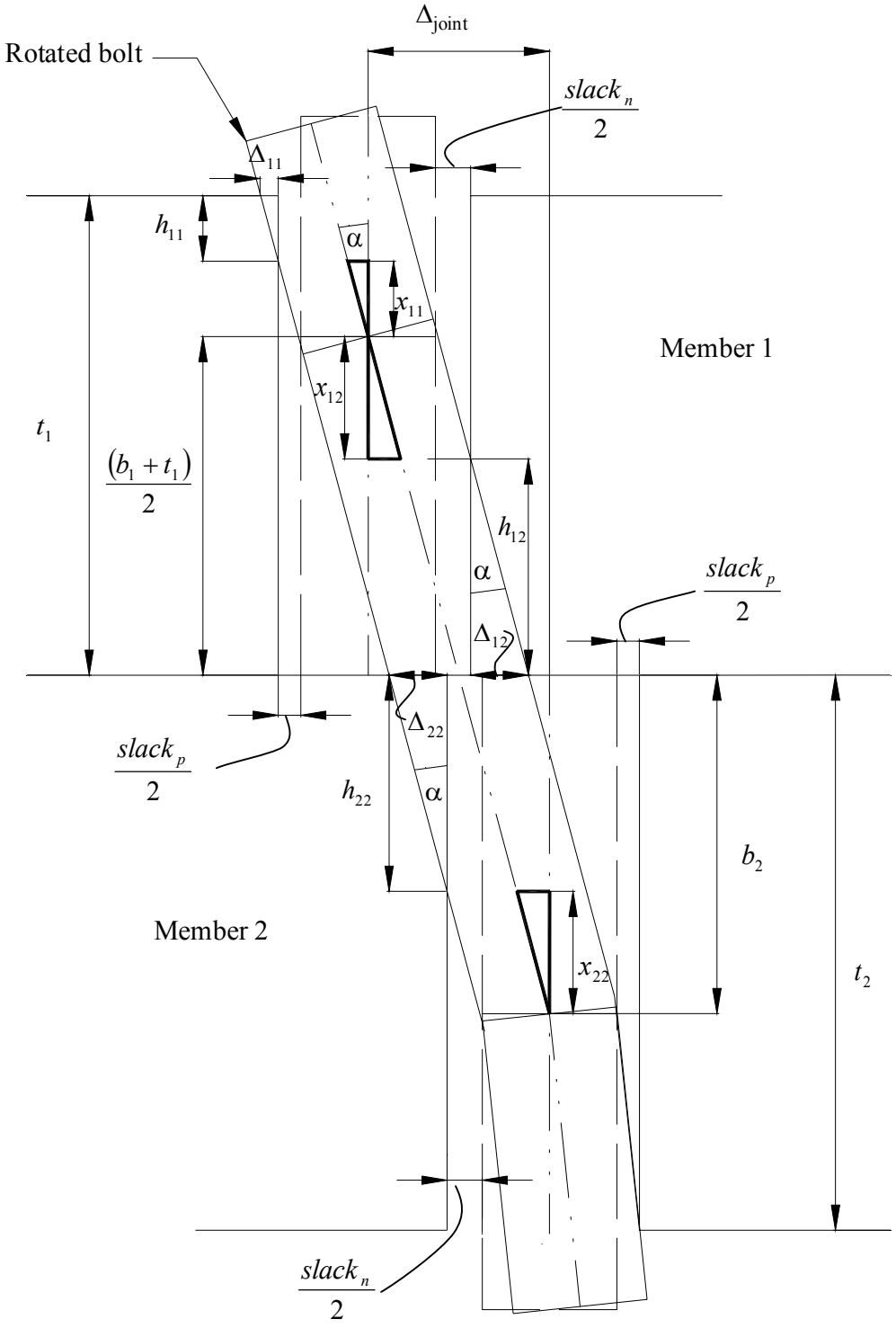

Figure 8.9: Bolt yielding in Mode III. Dimensions shown are used to compute the displaced volumes.

8.2.2.2.4 Mode IV

Since a plastic hinge forms in each member, the four volumes displaced are expressed by (Figure 8.10)

$$V_{perp,i2} = h_{i2} \cdot \overline{A}_{perp}(\hat{\Delta}_{i2}) \tag{8.43}$$

$$V_{para,i2} = h_{i2} \cdot \overline{A}_{para}(\hat{\Delta}_{i2}) \tag{8.44}$$

with

$$h_{i1} = b_i - x_{i2} \tag{8.45}$$

and

$$i = 1,2 \tag{8.46}$$

again, x_{ik} and $\hat{\Delta}_{ik}$ are as defined in Equation (8.27). The tangent of the rotation angle α is now defined as

$$\tan\alpha = \frac{\left|\Delta_{\text{joint}}\right|}{b_1 + b_2} \tag{8.47}$$

and in combination with Equation (8.33) and the Yield Theory, we find for b_1

$$b_1 = \sqrt{\frac{2 \cdot M_{yield}}{d_{bolt} \cdot \overline{F}_{embed}}} \tag{8.48}$$

		Units
t_i	thickness of Member *i*	mm
Δ_{joint}	total joint displacement	mm
Δ	Distance between bolt hole center and bolt center	mm
$slack_n$	total slack in negative displacement direction	mm
$slack_p$	total slack in positive displacement direction	mm
$F_{embed,i}$	embedment strength of Member *i*	kN/mm^2
$\overline{F}_{embed}$	Average embedment strength of both members	kN/mm^2
os	bolt hole oversize	mm
M_{yield}	yield moment of bolt in bending	kN m

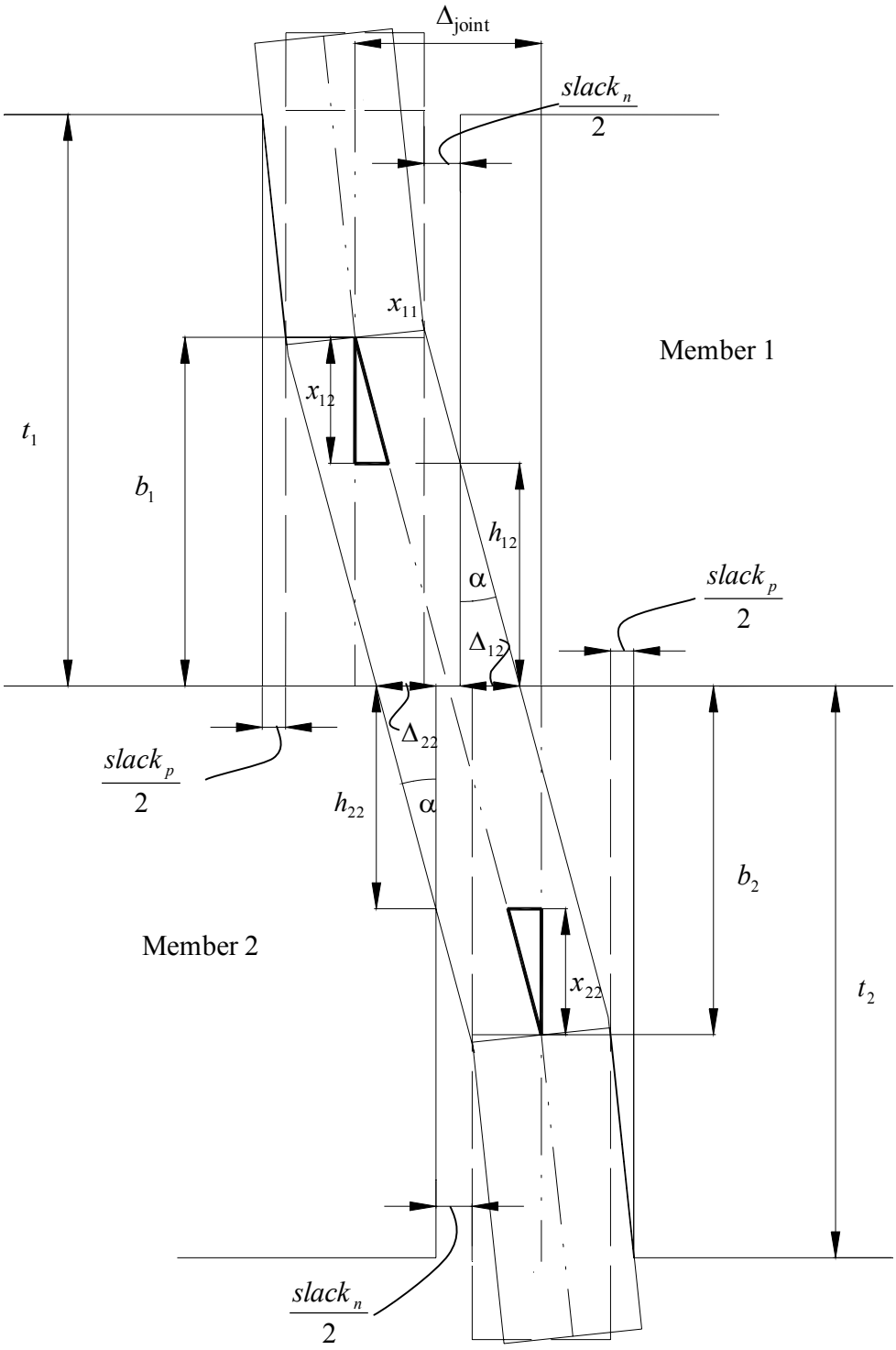

Figure 8.10: Bolt yielding in Mode IV. Dimensions shown are used to compute the displaced volumes.

8.2.2.3 Adjustment Factors

Displaced volumes were computed based on the assumption that the bolt cross section remains circular if viewed in the shear plane when, in fact, the cross section is an ellipse whose main axis elongates with increasing rotation angle α. This assumption introduces two errors. First, the computed strain area is smaller than the actual strain area and second, the calculated heights h_{ik} are shorter than actual, resulting in a displaced volume that is too small. To rectify the problem and diminish the error, two adjustment factors are introduced (obviously, the factors are not applied to Mode I yield).

Examine Figure 8.11. The elliptic area is related to the circular area by

$$a = \frac{r_{bolt}}{\cos\alpha} \tag{8.49}$$

$$A_{ellipse} = \pi ab = \pi \frac{\left(r_{bolt}\right)^2}{\cos\alpha} = \frac{1}{\cos\alpha} A_{circle} \tag{8.50}$$

Furthermore, we can write

$$h^* = r_{bolt} \cdot \sin\alpha \cdot \frac{1}{2} \tag{8.51}$$

Thus, the adjusted displaced volume (parallel or perpendicular, all modes except Mode I) is found to be

$$V = \overline{A}\left(\hat{\Delta}\right) \cdot \left(h + \frac{d_{bolt}}{4} \sin\alpha \right) \frac{1}{\cos\alpha} \tag{8.52}$$

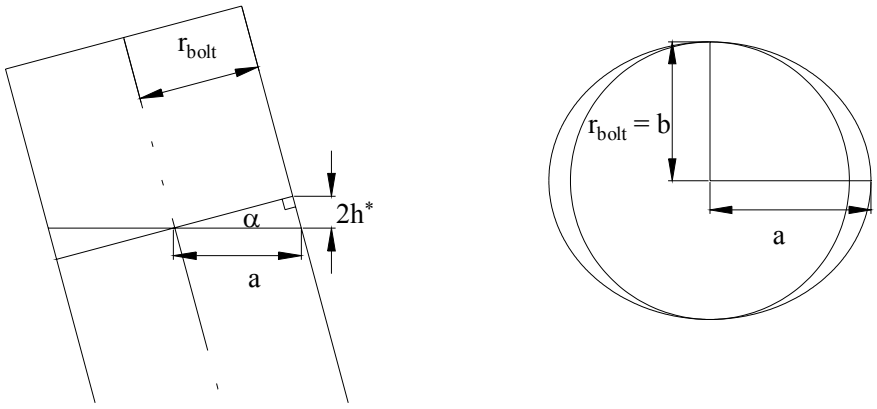

Figure 8.11: Because of rotation, bolt cross section is an ellipse when viewed in the shear plane. The elliptic cross section increases the strain area and the displaced volume height.

Note that the error is not completely compensated for because the strain area derived is a segment rather than a sector of a circle, and the proportionality to an elliptic area is only approximate.

8.2.3 Force Computation

If it is assumed that the wood foundation resembles a Winkler foundation in that it is an array of linear independent springs, then the same displaced volume always produces the same reactive force, no matter what the projected area is. To account for nonlinear deformations perpendicular and parallel to the grain, the nonlinearity factor Ω, is introduced as depicted in Figure 8.12. Furthermore, the ratio of E_{para} to E_{perp} is assumed fixed at (Bodig and Jayne 1982 Table 3.3; P. 116. E_L = 1.5; determined by taking the average of E_T and E_R)

$$\frac{E_{para}}{E_{perp}} = 15 \tag{8.53}$$

and the ratio of E_{para} to G_{para} is assumed as (Bodig and Jayne 1982 P. 156)

$$\frac{E_{para}}{G_{para}} = 16 \tag{8.54}$$

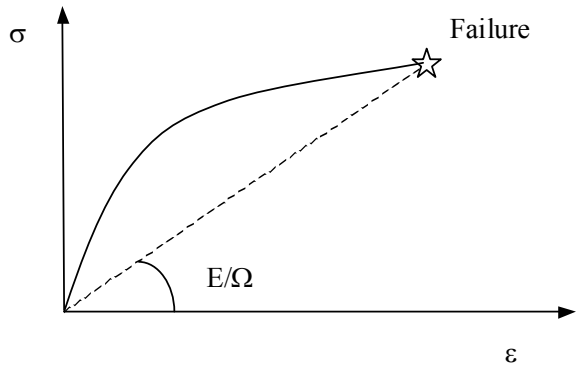

Figure 8.12: A nonlinearity factor effectively reduces the E modulus to account for plastic deformations.

		Units
E	modulus of elasticity	kN/mm^2
E_{para}	modulus of elasticity parallel to the grain	kN/mm^2
E_{perp}	modulus of elasticity perpendicular to the grain	kN/mm^2
Ω	nonlinearity factor	
G_{para}	shear modulus parallel to the grain	kN/mm^2

A general expression to determine the reactive force may be written as

$$F_{reaction} = \hat{\mathrm{K}} \cdot V_{displaced} \tag{8.55}$$

where,

$$\hat{\mathrm{K}} \quad \left[\frac{kN}{mm^3}\right] = \text{ pseudo foundation modulus} \tag{8.56}$$

8.2.3.1 Pseudo Foundation Modulus Perpendicular to the Grain

The pseudo foundation modulus perpendicular to the grain is modeled as a composite of both local and global stiffness effects to include the impact of changing member width relative to fastener diameter. Global stiffness effects are obtained based on beam-on-elastic-foundation theory.

Recall that beneath a bolt pressed into a wood foundation, two cracks are likely to develop a distance δ apart as described by Equation (8.1). The parts of the member outside the crack plane may be assumed to act like semi-infinite beams on elastic foundation since in a single shear joint, one member end may be relatively close to the bolt hole without violating end distance requirements (Figures 8.13 and 14)[2].

Let *z* be the beam axis and let the origin of the coordinate system (*z, y*) be at the point of force application (Figure 8.14). Then the formula for the displacement distribution *y(z)* of a semi-infinite beam may be found to be (Boresi et al.1993)

$$y(z) = \frac{F_{perp} \cdot \beta}{2 \cdot h_{ik} \cdot \mathrm{K}^*} \cdot \left(A_{\beta|z|} + 2 \cdot D_{\beta a} \cdot D_{\beta(a+z)} + C_{\beta a} \cdot C_{\beta(a+z)}\right), \qquad z \geq -a \tag{8.57}$$

with

[2] Jorissen (1998) investigated double shear joints and computed stresses perpendicular to the grain by assuming a finite beam on elastic foundation in combination with fracture mechanics. See Section 3.3.3

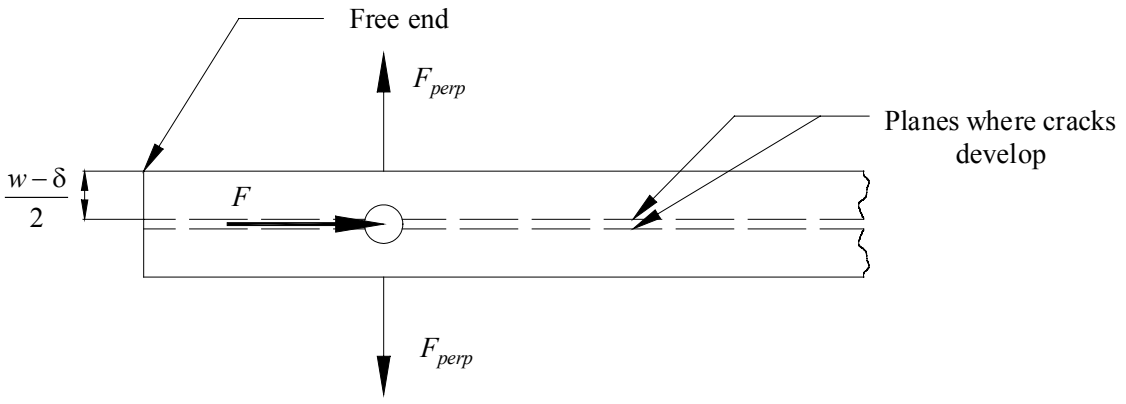

Figure 8.13: The figure shows the planes where cracks are likely to develop as determined by Jorissen (1998). The parts of the member outside the two crack planes are modeled as semi-infinite beams on elastic foundation subjected to F_{perp} which is the force perpendicular to the grain caused by the bolt subjected to F.

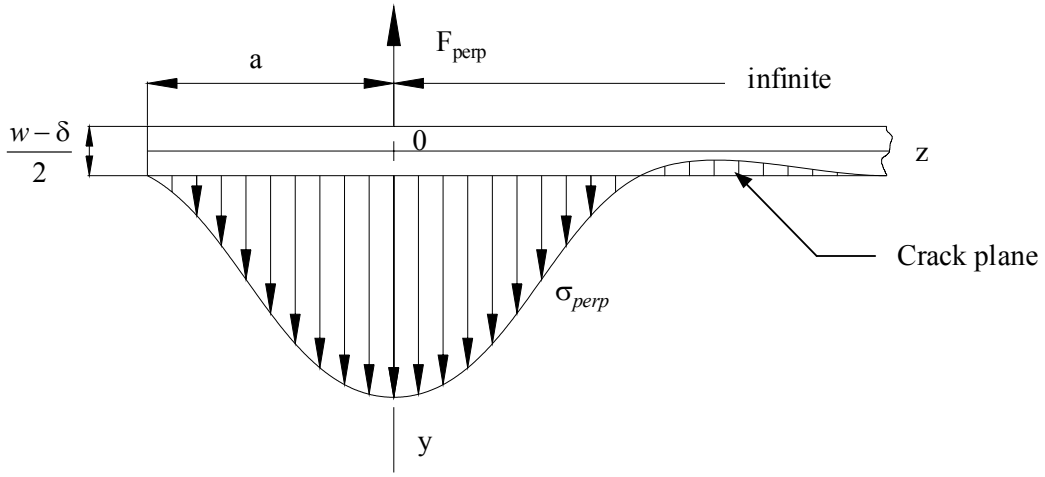

Figure 8.14: Stress distribution along a semi-infinite beam on elastic foundation subjected to a point load, F_{perp} a distance of a away from the end.

$$A_{\beta z} = e^{-\beta \cdot z} \cdot \left(\sin\left[\beta|z|\right] + \cos\left[\beta|z|\right]\right) \tag{8.58}$$

$$C_{\beta a} = e^{-\beta \cdot a} \cdot \left(\cos\left[\beta \cdot a\right] - \sin\left[\beta a\right]\right) \tag{8.59}$$

$$C_{\beta(a+z)} = e^{-\beta \cdot (a+z)} \cdot \left(\cos\left[\beta \cdot (a+z)\right] - \sin\left[\beta \cdot (a+z)\right]\right) \tag{8.60}$$

$$D_{\beta a} = e^{-\beta \cdot a} \cdot \left(\cos\left[\beta \cdot a\right]\right) \tag{8.61}$$

$$D_{\beta(a+z)} = e^{-\beta \cdot (a+z)} \cdot \left(\cos\left[\beta \cdot (a+z)\right]\right) \tag{8.62}$$

$$\beta = \left(\frac{h_{ik} \cdot \mathrm{K}^*}{4 \cdot E_{para} \cdot I_{para}} \right)^{\frac{1}{4}} \tag{8.63}$$

and the moment of inertia, I_{para}, is defined as

$$I_{para} = \frac{h_{ik} \cdot \left(\frac{w - \delta}{2} \right)^3}{12} \tag{8.64}$$

w denotes the width of the side member, δ is the distance between the two cracks and h_{ik} is the height of the corresponding displaced volume as defined in the preceding section. From the foregoing, it is clear that the semi-infinite beam is not assumed to be as wide as the side member is deep but its width equals the height of the respective volume displaced. However, since a three dimensional Winkler foundation is assumed, beam width eventually cancels out. K^* is the three-dimensional foundation modulus, which characterizes the beam's foundation by

$$\mathrm{K}^* = \frac{E_{perp}}{\frac{\delta}{2}} \tag{8.65}$$

Because of symmetry, the line of zero strain perpendicular to the grain in the member coincides with the bolt center, which is also the center between the two cracks. Therefore, the foundation for each beam is $\delta / 2$ deep.

The goal is to find the global stiffness at the bolt location where $z = 0$. Hence, rearranging Equation (8.57) to solve for F_{perp} yields

$$F_{perp} = K_g \cdot y(0) \tag{8.66}$$

and upon substitution and simplification the global stiffness, K_g, is

$$K_g = \frac{2 \cdot E_{para} \cdot h_{ik}}{3 \cdot 5^{0.75} \cdot \vartheta^{0.25} \cdot \left(\delta + \delta \cdot e^{-\xi} \cdot \left(2 + \cos(\xi) - \sin(\xi)\right)\right)} \tag{8.67}$$

with

$$\vartheta = \frac{1}{\delta \cdot (w - \delta)^3} \tag{8.68}$$

and

$$\xi = \frac{4 \cdot a \cdot \vartheta^{0.25}}{5^{0.25}} \tag{8.69}$$

If the semi-infinite beam is very deep (i.e. the side member is very wide), the bolt will indent it rather than bend it. Hence, to account for local effects, the global stiffness is arranged in series with the material (local) stiffness. Assume the bolt-member interaction can be abstracted as portrayed in Figure 8.15. Observe that springs of length L_2 are arranged in parallel. Yet, spring of length L_1 is in series with both springs of length L_2. From this, the local stiffness may be expressed as

$$K_l = \frac{E_{perp}}{L_1 + \frac{L_2}{2}} \tag{8.70}$$

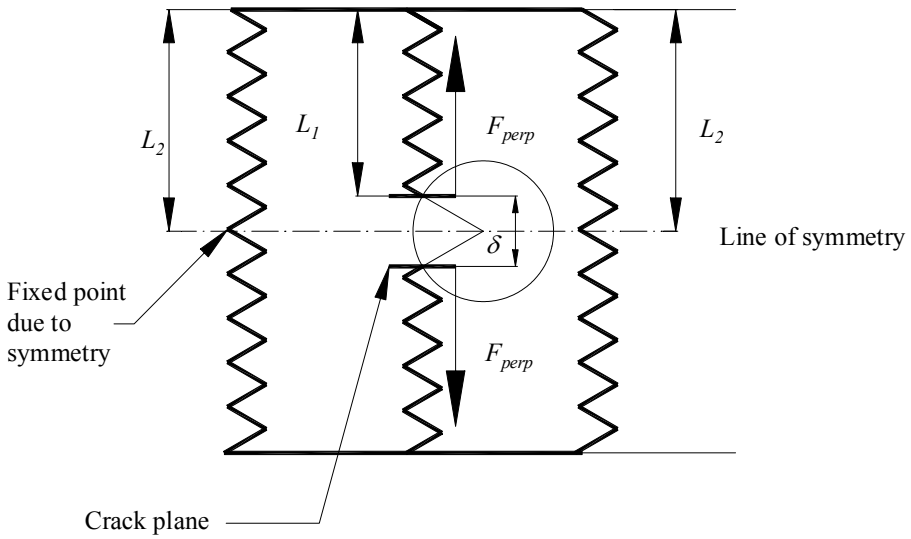

Figure 8.15: Abstraction of local bolt-member interaction.

Based on the foregoing, the pseudo-foundation modulus perpendicular to the grain is found to be

$$\hat{\mathrm{K}}_{perp} = \left[\frac{1}{K_g} + \frac{1}{K_l}\right]^{-1} \cdot \frac{1}{h_{ik} \cdot \frac{\Delta_{ik}}{2}} \tag{8.71}$$

		Units
E_{para}	modulus of elasticity parallel to the grain	kN/mm^2
E_{perp}	modulus of elasticity perpendicular to the grain	kN/mm^2
a	end distance	mm
δ	distance between the two cracks as described by eq. (8.1)	mm
z	distance along beam axis	mm
y	beam deflection	mm
w	side member width	mm
h_{ik}	height of displaced volume as defined in Sec. 8.2.2.2	mm
Δ_{ik}	displacement as defined in Sec. 8.2.2.2	mm
K_g	global stiffness obtained at z = 0	kN/mm
K_l	local stiffness	kN/mm
K^*	three-dimensional foundation modulus describing the beam foundation	kN/mm^3
F_{perp}	force perpendicular to the grain exerted by the bolt	kN
σ	stress perpendicular to the grain	kN/mm^2
I_{para}	moment of inertia about axis parallel to bolt axis	mm^4
L_i	length	mm

8.2.3.2 Pseudo Foundation Modulus Parallel to the Grain

The pseudo foundation modulus parallel to the grain takes into account the shear strain distribution along the crack planes. While the derivation and its result that follow are different, the starting point leans on the approach presented earlier by Jorissen (1998). If a bolt is laterally loaded, the surrounding wood counteracts the load, and ideally, forces are shared equally on either side of the bolt due to symmetry. Key to deriving the foundation modulus is the insight that forces parallel to the grain act across the area of the segment between the crack planes. Moreover, the summation of shear stress over the crack plane area between two bolts, or between a bolt and a member free end, counteracts the force parallel to the grain. Consider the section of infinitesimal small length, *dz* in Figure 8.16. To satisfy equilibrium, we can write

$$dF_1 = \tau \cdot dz \cdot t = -dF_2 \tag{8.72}$$

or

$$\frac{dF_1}{dz} - \tau \cdot t = 0 \tag{8.73}$$

Using strain-displacement relations we find

$$\varepsilon_1 = \frac{du_1}{dz} = \frac{2 \cdot dF_1}{E_{para} \cdot A_m} \quad \Leftrightarrow \quad du_1 = \frac{2 \cdot dF_1}{E_{para} \cdot A_m} \cdot dz \tag{8.74}$$

$$\varepsilon_2 = \frac{du_2}{dz} = -\frac{dF_2}{E_{para} \cdot A_s} \quad \Leftrightarrow \quad du_2 = -\frac{dF_2}{E_{para} \cdot A_s} \cdot dz \tag{8.75}$$

$$\gamma = \frac{2 \cdot \left(du_1 - du_2\right)}{\delta} \tag{8.76}$$

where A_m and A_s are the cross sectional areas of the section between the crack planes and the part of the member with width equal to *h,* respectively (Figure 8.16). Substituting Equations (8.74) and (8.75) into Equation (8.76) and taking the second derivative yields

$$\frac{d^2\gamma}{dz^2} = \frac{2}{\delta} \cdot \frac{dF_1}{dz} \cdot \left[\frac{2}{E_{para} \cdot A_m} + \frac{1}{E_{para} \cdot A_s} \right] \tag{8.77}$$

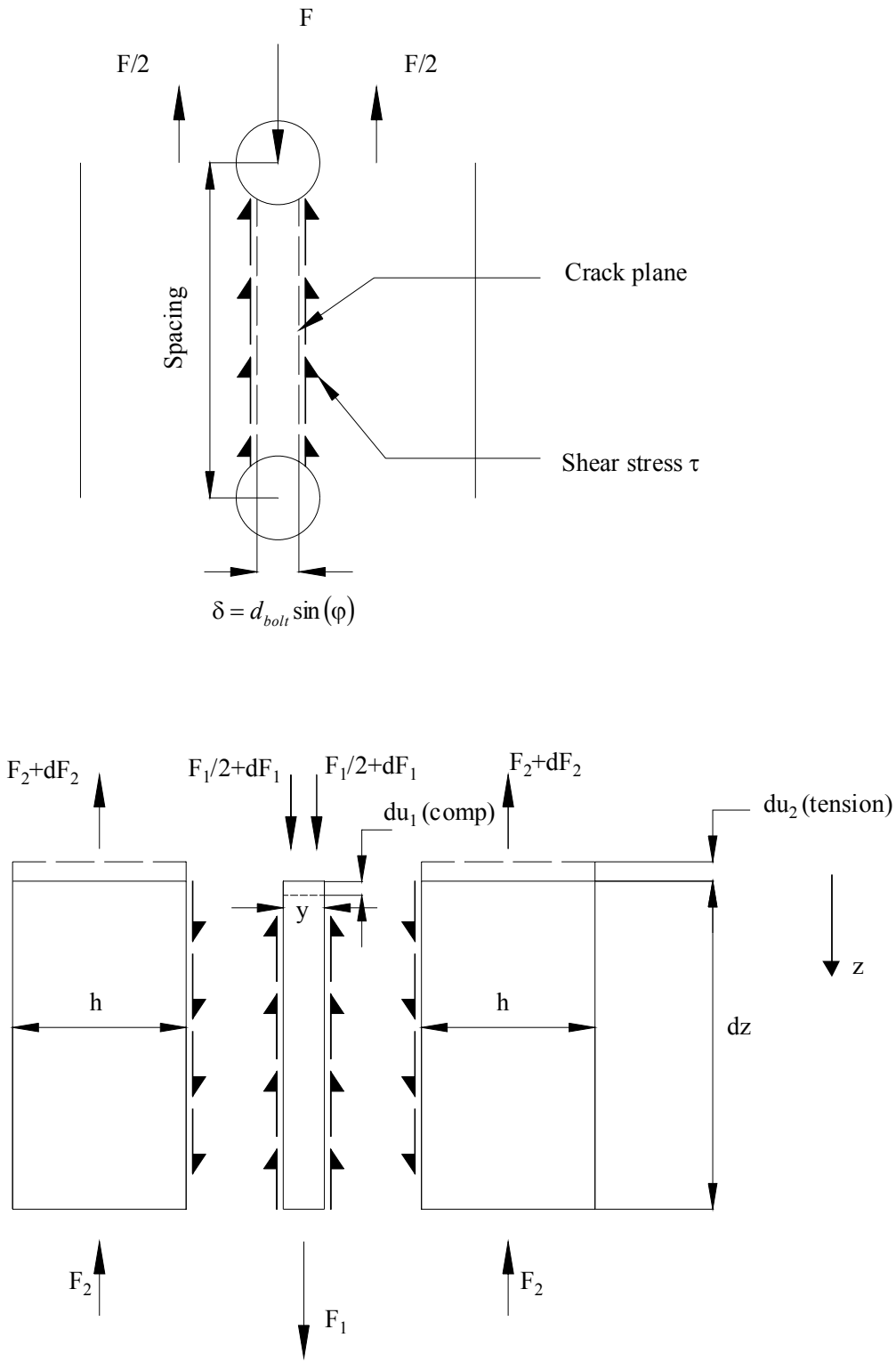

Figure 8.16: Shear stress along the crack planes and free body diagram of a section of infinitesimal small length.

But considering Equation (8.73), it can be found that

$$\frac{d^2\gamma}{dz^2} = \frac{2}{\delta}\cdot\left(\tau\cdot t\cdot\left[\frac{2}{E_{para}\cdot A_m}+\frac{1}{E_{para}\cdot A_s}\right]\right) = \gamma\cdot\left[\frac{4\cdot t\cdot G_{para}}{E_{para}\cdot A_m\cdot\delta}+\frac{2\cdot t\cdot G_{para}}{E_{para}\cdot A_s\cdot\delta}\right] = \gamma\cdot\omega^2 \tag{8.78}$$

with

$$\omega^2 = \frac{4\cdot t\cdot G_{para}}{E_{para}\cdot A_m\cdot\delta}+\frac{2\cdot t\cdot G_{para}}{E_{para}\cdot A_s\cdot\delta} \qquad \left[\frac{1}{mm^2}\right] \tag{8.79}$$

Hence, the shear strain distribution may be described by the following ordinary differential equation of second order

$$\frac{d^2\gamma}{dz^2}-\gamma\cdot\omega^2 = 0 \tag{8.80}$$

with the solution

$$\gamma(z) = A\cdot e^{-z\cdot\omega}+B\cdot e^{z\cdot\omega} \tag{8.81}$$

Coefficients *A* and *B* are determined by boundary conditions. Attributed to bolt-hole oversize, the section between the crack planes has one loaded and one unloaded (free) surface, each being part of a bolt hole. Thus, if *z* is the axis parallel to the grain, pointing in the direction of loading, whose origin is d_{bolt} / *2* away from the bolt center in the direction of loading, we find at $z = 0$

$$\varepsilon_1 = \frac{F}{E_{para}\cdot A_m};\quad \varepsilon_2 = -\frac{F}{2\cdot E_{para}\cdot A_s} \tag{8.82}$$

and with use of the first derivatives of Equation (8.76) and Equation (8.81) we arrive at

$$\frac{d\gamma}{dz} = \frac{2}{\delta}\left(\frac{F}{E_{para}\cdot A_m}+\frac{F}{2\cdot E_{para}\cdot A_s}\right) = -A\cdot\omega\cdot e^{-0\cdot\omega}+B\cdot\omega\cdot e^{0\cdot\omega} \tag{8.83}$$

The free end at $z = L = s - d_{bolt}$, where *s* denotes fastener spacing, imposes the condition

$$dF_1 = dF_2 = 0 \tag{8.84}$$

which results in

$$\frac{d\gamma}{dz} = 0 = -A \cdot \omega \cdot e^{-L \cdot \omega} + B \cdot \omega \cdot e^{L \cdot \omega} \tag{8.85}$$

Note that the effect of bolt diameter is included. From the foregoing, coefficients A and B are defined as

$$A = B \cdot e^{2 \cdot L \cdot \omega} \tag{8.86}$$

$$B = \frac{A_m \cdot F + 2 \cdot A_s \cdot F}{A_m \cdot A_s \cdot E_{para} \cdot \delta \cdot \omega - \left(A_m \cdot A_s \cdot E_{para} \cdot \delta \cdot \omega\right) \cdot e^{2 \cdot L \cdot \omega}} \tag{8.87}$$

To find the pseudo foundation modulus parallel to the grain, we substitute γ in Equation (8.81) by Equation (8.76), solve for du_1, and obtain, using the relations expressed in Equations (8.74) and (8.75),

$$du_1 = \frac{1}{2 \cdot \left(1 + \frac{A_m}{A_s}\right)} \left(A \cdot e^{-z \cdot \omega} + B \cdot e^{z \cdot \omega}\right) \cdot \delta \tag{8.88}$$

coefficients A and B are as defined in Equations (8.86) and (8.87). Let

$$A_m = h_{ik} \cdot \delta \tag{8.89}$$

and

$$A_s = h_{ik} \cdot \left(\frac{w - \delta}{2}\right) \tag{8.90}$$

with h_{ik} defined as in Section 8.2.2.2 and w denoting side member width. At $z = 0$, substitution and isolation of F yields by consideration of the sign convention

$$F = K_{para} \cdot du_1 \tag{8.91}$$

and K_{para} is defined as

$$K_{para} = \frac{2 \cdot E_{para} \cdot h_{ik} \cdot \sqrt{\frac{G_{para} \cdot w}{E_{para}\left(w - \delta\right) \cdot \delta^2}} \cdot \delta \cdot \left(w + \delta\right) \cdot \tanh\left[2 \cdot L \sqrt{\frac{G_{para} \cdot w}{E_{para}\left(w - \delta\right) \cdot \delta^2}}\right]}{w} \tag{8.92}$$

The pseudo foundation modulus is obtained by dividing K_{para} by $A_m + A_s$ and the factor $(1+A_m/A_s)$ to account for the fact that due to relative motion the total displacement is $du_1 + du_2$. Thus, simplification yields

$$\hat{K}_{para} = \frac{4 \cdot G_{para} \cdot \tanh\left[2 \cdot L \cdot \sqrt{\frac{G_{para} \cdot w}{E_{para} \cdot (w-\delta) \cdot \delta^2}}\right]}{\sqrt{\frac{G_{para} \cdot w}{E_{para} \cdot (w-\delta) \cdot \delta^2}} \cdot \delta \cdot (w+\delta)} \tag{8.93}$$

		Units
E_{para}	modulus of elasticity parallel to the grain	kN/mm^2
G_{para}	shear modulus parallel to the grain	kN/mm^2
ε_i	normal strain	
γ	shear strain	
A_m	cross sectional area of segment between crack planes	mm^2
A_s	cross sectional area of part of side member outside the two crack planes.	mm^2
d_{bolt}	bolt diameter	mm
δ	distance between the two cracks as described by eq. (8.1)	mm
w	side member width	mm
h	(w-δ) / 2	
h_{ik}	height of displaced volume as defined in Sec. 8.2.2.2	mm
F	force parallel to the grain exerted by the bolt	kN
s	spacing between two bolts or bolt and free member end	mm
L	s - d_{bolt}	mm
t	side member thickness	mm

8.2.3.3 Summation of Forces

With the pseudo foundation moduli derived in the preceding sections, it is now possible to compute the reaction force caused by a displaced volume. Each bolt displaces several volumes and hence causes more than one reaction force. The number of volumes displaced per bolt changes depending on yield mode. To compute failure stresses, the reaction forces obtained are added or subtracted based on their direction of application.

Perpendicular to grain reaction forces all act in the same direction and are therefore added (in this case, due to symmetry, only half of the joint cut perpendicular to the shear plane is considered). Thus, the total force perpendicular to the grain produced per bolt and member is obtained by

$$F_{perp,i} = \sum_{k=1}^{n} F_{perp,ik} \tag{8.94}$$

where *i* denotes the member number and *n* equals 1 or 2, subject to yield mode.

Attributed to their different directions and interactions, parallel to the grain forces (used to computed shear stresses) for each segment between bolts or between a bolt and a member end are computed by (Figure 8.17)

$$\begin{aligned} F_{para1(shear),member1} &= -F_{para11(shear),bolt1} \\ F_{para2(shear),member1} &= F_{para12(shear),bolt1} - F_{para11(shear),bolt2} \end{aligned} \tag{8.95}$$

for Member 1 and negative direction of movement. Other forces are obtained accordingly. Clearly, depending on yield mode, some forces depicted in Figure 8.17 may be zero. It is noteworthy that parallel forces computed for member segments between two bolts are equal to the net force on the bolt as revealed in Figure 8.1. However, for Modes II and III, parallel to grain forces are higher than the net force in the segments between the member ends and the bolt, increasing splitting potential at that location.

Negative direction of movement:

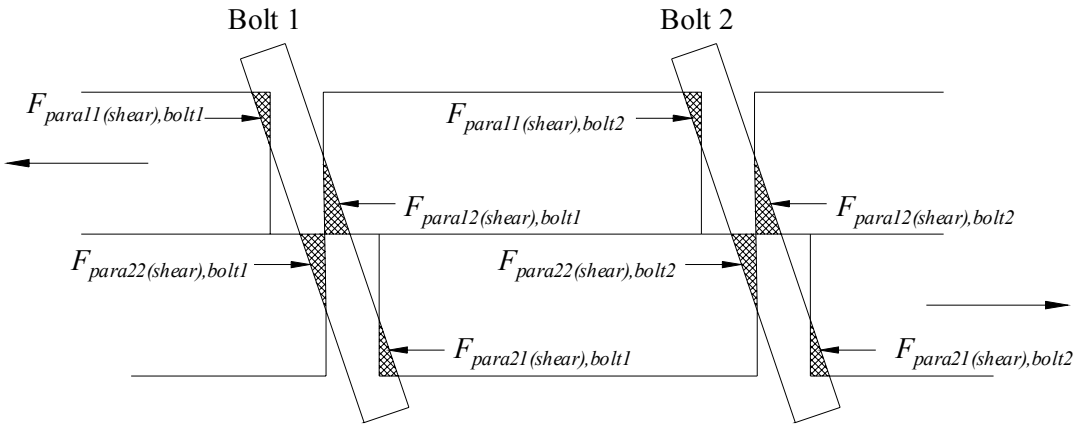

Positive direction of movement:

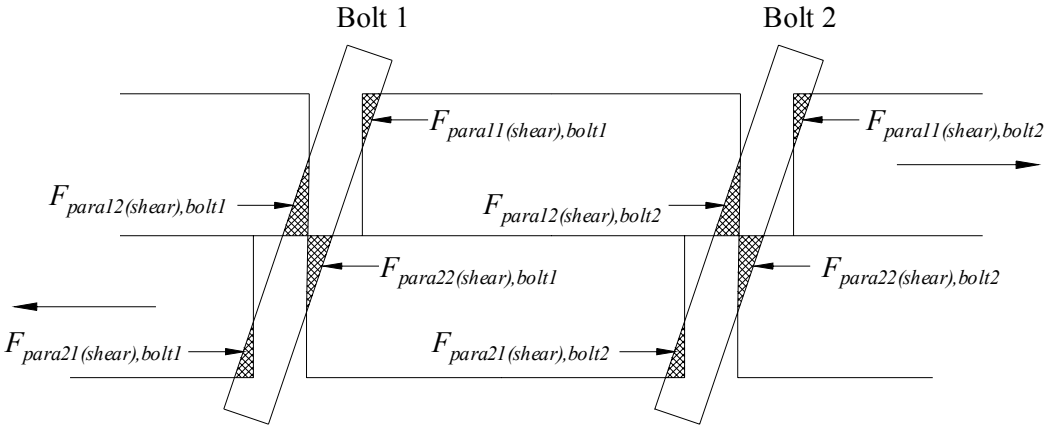

Figure 8.17: Example joint (Mode II) to demonstrate the direction and consequent summation of forces parallel to the grain caused by displaced volumes (shaded areas).

8.3 Stress Distributions

Shear and perpendicular to grain stresses are identified in the crack planes because it is assumed that failure occurs at this location (Figure 8.14). As elaborated in previous sections, catastrophic failure is primarily due to a combination of perpendicular to grain stress and shear stress. Stresses do not act independently, however, which means that normal stress parallel to the grain needs to be accounted for as well.

8.3.1 Perpendicular to Grain Stress

Based on the same assumptions as employed to derive the foundation modulus perpendicular to the grain, stresses perpendicular are obtained using semi-infinite beam on elastic foundation theory and the principle of superposition to account for multiple fasteners. To simplify the analysis, the influence of the bolt hole on the foundation is neglected, since beam length >> bolt hole diameter. It is important to realize that unlike the force computed with the displaced volume method, the sum of the stresses perpendicular to the grain over the beam length is not affected by the foundation modulus. This must be true to satisfy equilibrium. A lower modulus produces greater displacements at a given force and hence the sum of the stresses does not change. However, the same is not true for stress distribution. Stress distribution changes as the foundation modulus relative to beam stiffness changes. Consequently, with reference to Figure 8.14, the stress distribution perpendicular to the grain for a single bolt joint may be obtained by

$$\sigma(z) = \frac{F_{perp} \cdot \beta}{2 \cdot t_i} \left(A_{\beta|z|} + 2 \cdot D_{\beta a} \cdot D_{\beta(a+z)} + C_{\beta a} \cdot C_{\beta(a+z)} \right), \quad z \geq -a \tag{8.96}$$

where t_i is the thickness of Member i, z is the longitudinal member axis with origin at the free member end, and all other parameters are as defined in Section 8.2.3.1.

If a joint holds a total of *nbolt* bolts, the stress distribution of each fastener is superimposed along the length of the joint member such that

$$\sigma(z)_{total} = \sum_{j=1}^{nbolt} \frac{F_{perp,j} \cdot \beta_j}{2 \cdot t_i} \left(A_{\beta|z|,j} + 2 \cdot D_{\beta a,j} \cdot D_{\beta(a+z),j} + C_{\beta a,j} \cdot C_{\beta(a+z),j} \right), \quad z \geq -a \tag{8.97}$$

Although Equation (8.97) describes a continuous function, MULTBOLT computes stresses at discrete points. This is due to the fact that the stress function must be integrated to determine failure (see Sec. 8.4). Yet the integral of Equation (8.97) can only be obtained numerically for which a list of discrete values greatly simplifies the process. MULTBOLT allows the grid resolution to be selected at will. However, high resolutions (i.e. length increments << 1mm) considerably increase computing time and rounding error because the program must loop through the grid for each time step. Figure 8.18 shows the stresses for each individual bolt, and the resulting total stress as computed by MULTBOLT, for a three fastener joint at 1 mm increments. Negative stress is compression stress and round dots indicate bolt locations. The distribution shown is a smooth function. To keep the analysis reasonably simple, no peak stresses attributed

to stress concentrations that develop at crack tips or around discontinuities such as bolt holes are included. However, since the failure criterion presented in Section 8.4 takes crack development and crack growth into account, the inclusion of peak stresses may not be necessary.

If slack is equal in positive and negative directions of movement, perpendicular to grain stresses are not affected by the direction of movement, only by the displacement level.

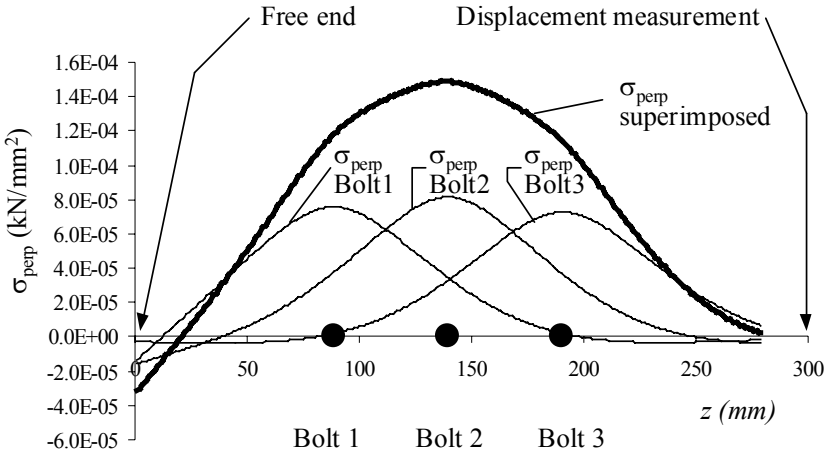

Figure 8.18: Stresses perpendicular to the grain of individual bolts and superimposed stress as computed by MULTBOLT along the member axis *z* for a three-bolt joint. Stresses shown were computed at a single time step with constant displacement (< failure displacement), Mode II yield, symmetric slack of 0.8 mm in either direction, southern pine members 140 x 38 mm^2, and 12.7 mm bolt diameter.

8.3.2 Shear Stresses

Shear stresses are computed based on the shear strain distribution expressed in Equation (8.81) and the relationship of stress and strain.

$$\tau(z) = G_{para} \cdot \left(A \cdot e^{-z \cdot \omega} + B \cdot e^{z \cdot \omega} \right) \tag{8.98}$$

where z is the longitudinal member axis and

$$A = B \cdot e^{2 \cdot L \cdot \omega} \tag{8.99}$$

$$B = \frac{A_m \cdot F + 2 \cdot A_s \cdot F}{A_m \cdot A_s \cdot E_{para} \cdot \delta \cdot \omega - \left(A_m \cdot A_s \cdot E_{para} \cdot \delta \cdot \omega \right) \cdot e^{2 \cdot L \cdot \omega}} \tag{8.100}$$

with

$$\omega^2 = \frac{4 \cdot t \cdot G_{para}}{E_{para} \cdot A_m \cdot \delta} + \frac{2 \cdot t \cdot G_{para}}{E_{para} \cdot A_s \cdot \delta} \qquad \left[\frac{1}{mm^2}\right] \tag{8.101}$$

as defined previously. Given that bolt diameter may be as much as 25 percent of minimum fastener spacing (minimum spacing requirement for full capacity according to NDS 1999), the effect of bolt hole diameter is included. Similar to the pseudo foundation modulus, stresses parallel to the grain are computed along the length

$$L = s - d_{hole} \tag{8.102}$$

rather than using spacing, *s*. Thus, the shear stress distribution per 1 mm segment as depicted in Figure 8.19 is zero around the bolt locations. Figure 8.19 reveals the shear stress distribution of Member 1, for positive and negative displacements and bolts yielding in Mode II. Observe that for positive displacement, Bolt 1 causes higher shear stresses than the other two bolts. In addition, Bolt 3 produces positive and negative shear stresses. This is only true for Modes II and III. The reason is that while for Mode II and III forces subtract in intermediate segments as indicated in Section 8.2.3, the first and last bolts face no other bolt towards member end (see Figure 8.17). Hence, the higher stress is caused by F_{para12} of Bolt 1 and the negative stress is produced by F_{para11} of Bolt 3.

There is no interaction between the shear stresses caused by the individual fasteners. To see this, observe that the two crack planes shown in Figure 8.16 emanate from a bolt hole and end either at a bolt hole or a member end. Hence, the segments between the bolts and between a bolt and a member end are confined by two free ends and are thus completely isolated such that no shear forces are transferred to the next segment.

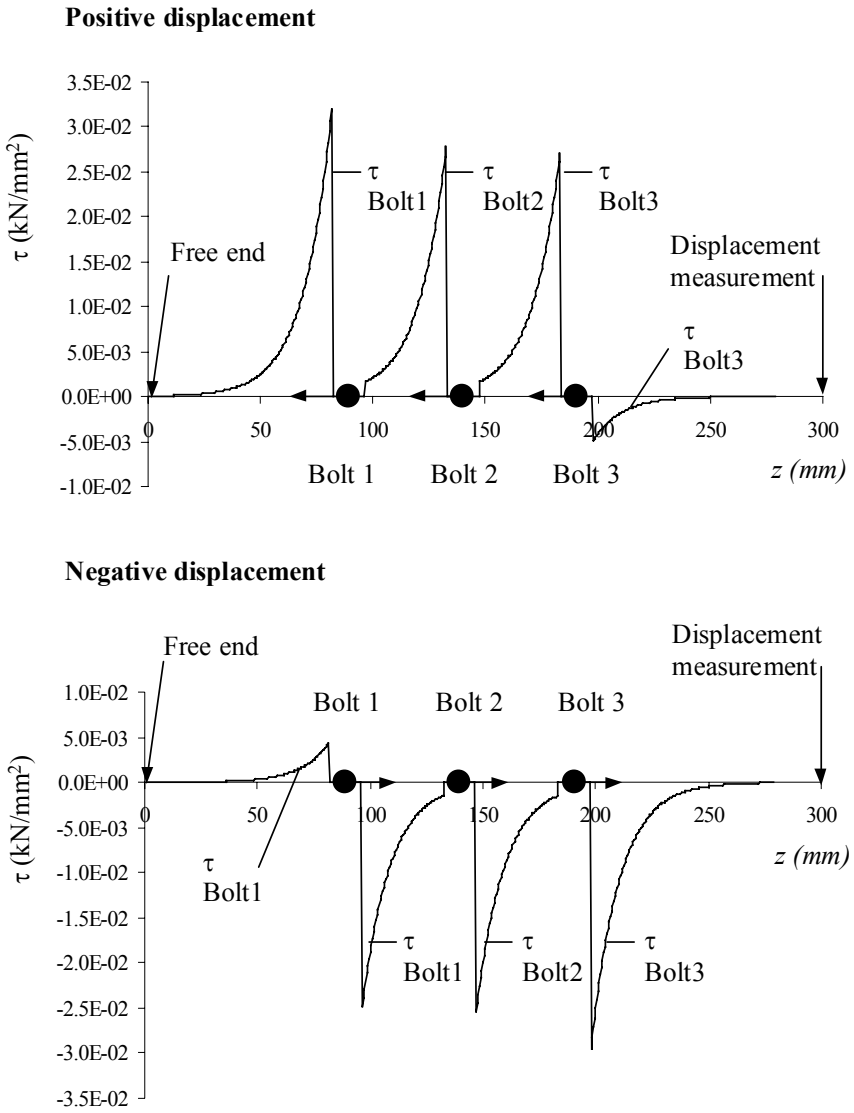

Figure 8.19: Shear stress distributions for positive and negative displacements, respectively, as computed by MULTBOLT. Stresses shown were computed at a single time step with large constant displacement, Mode II yield, symmetric slack of 0.8 mm in either direction, southern pine members 140 x 38 mm^2, and 12.7 mm bolt diameter.

8.3.3 Parallel to Grain Stresses

Parallel to grain stresses are computed based on the average normal force acting in the member within each segment. Thus, based on the joint layout convention revealed in Section 7.2, and Figure 8.20, we can write for Member 1

$$\sigma_{para,Member1,1} = 0.0 \tag{8.103}$$

and

$$\sigma_{para,Member1,j} = \frac{\sum_{i=2}^{j} F_i}{A_{Member1}} \tag{8.104}$$

with

$$j = 1,2,\cdots,nbolt+1 \tag{8.105}$$

nbolt denotes the total number of bolts in the joint, $A_{Member1}$ stands for the cross sectional area of Member 1,which is assumed to be constant (i.e. bolt holes are neglected), and j indicates the segment number. F_i specifies the force resisted by each bolt. Because Segment 1 in Member 1 is at the free end, no normal stresses exist. Accordingly, for Member 2 we find

$$\sigma_{para,Member2,nbolt} = 0.0 \tag{8.106}$$

and

$$\sigma_{para,Member2,j} = \frac{\sum_{i=j}^{1} F_i}{A_{Member2}} \tag{8.107}$$

with

$$j = nbolt+1, nbolt, nbolt-1,\cdots,1 \tag{8.108}$$

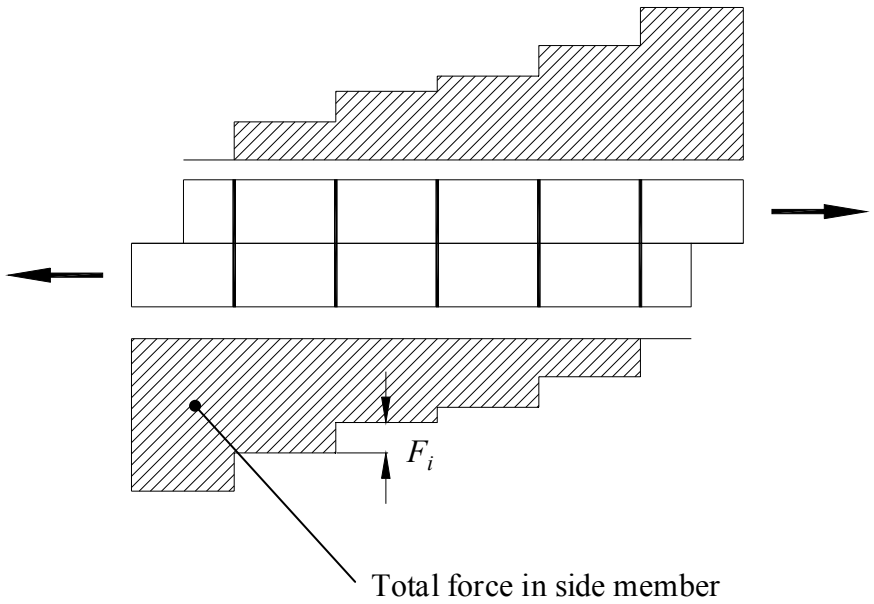

Figure 8.20: Distribution of normal forces per member. Forces add at each bolt location leading to a step-wise distribution.

Parallel to grain stress distribution is a stepwise function along the length of the member. Figure 8.21 shows the computed parallel to grain stresses for Member 1 in a three bolt joint with bolts yielding in Mode II for negative and positive displacements. Step size is not constant and depends on the resisted force at each bolt.

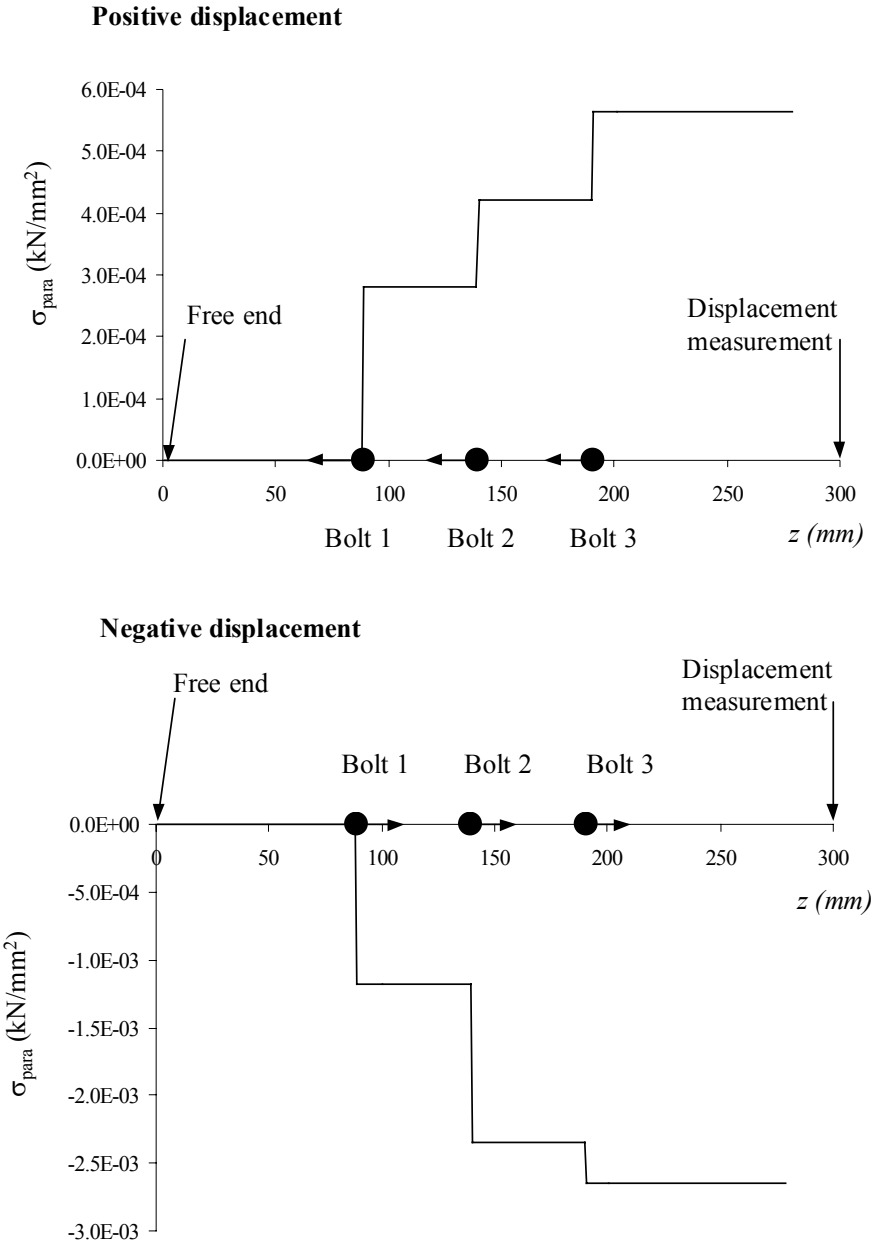

Figure 8.21: Parallel to grain stress distributions for positive and negative displacements, respectively, as computed by MULTBOLT. Stresses shown were computed at a single time step with large constant displacement, Mode II yield, symmetric slack of 0.8 mm in either direction, southern pine members 140 x 38 mm^2, and 12.7 mm bolt diameter. Note that negative displacement induces compression stress.

8.4 Modified Tsai-Wu Failure Criterion

It has long been suspected that stresses in principal directions influence each other and therefore affect material failure. Especially for fibrous materials, stress interaction may change failure mode and failure stress. For example, a compressive stress perpendicular to wood fibers may support the fibers, prevent buckling in longitudinal direction, and thus increase longitudinal compression strength, or shear stresses may limit tension perpendicular to the grain strength (Hyer 1997). The Tsai-Wu failure criterion is an interactive failure theory that has been used mostly for fiber reinforced materials and was derived from the well known von Mises criterion for isotropic materials.

Generally, for an orthotropic material, there are a total of nine failure stresses that have to be determined (six normal and three shear stresses) where a maximum of six stresses can be physically applied at once. In most cases, however, not all six stresses are applied simultaneously, as is true in this work. The stresses we are concerned with here are shear, tension or compression perpendicular, and tension or compression parallel to the grain. Based on the assumptions (Winkler foundation) and methods (DVM) used, the five stresses derived all act in the same plane permitting the plane-stress assumption and greatly reducing the complexity of the failure criterion. Hence, for the stresses considered here, the Tsai-Wu Criterion may be written as

$$C_1 \cdot \sigma_{para} + C_2 \cdot \sigma_{perp} + C_{11} \cdot \sigma_{para}^2 + C_{22} \cdot \sigma_{perp}^2 + C_{66} \cdot \tau^2 - \sqrt{C_{11} \cdot C_{22}} \cdot \sigma_{para} \cdot \sigma_{perp} = 1.0 \tag{8.109}$$

where

$$C_1 = \frac{1}{\sigma_{para}^T} + \frac{1}{\sigma_{para}^C} \tag{8.110}$$

$$C_2 = \frac{1}{\sigma_{perp}^T} + \frac{1}{\sigma_{perp}^C} \tag{8.111}$$

$$C_{11} = -\frac{1}{\sigma_{para}^T \cdot \sigma_{para}^C} \tag{8.112}$$

$$C_{22} = -\frac{1}{\sigma_{perp}^T \cdot \sigma_{perp}^C} \tag{8.113}$$

$$C_{66} = \left(\frac{1}{\tau^F} \right)^2 \tag{8.114}$$

		Units
σ_{perp}	stress perpendicular to the grain (tension or compression)	kN/mm^2
σ_{para}	stress parallel to the grain (tension or compression)	kN/mm^2
τ	shear stress	kN/mm^2
σ_{perp}^{T}	tensile strength perpendicular to the grain	kN/mm^2
σ_{perp}^{C}	compression strength perpendicular to the grain	kN/mm^2
σ_{para}^{T}	tensile strength parallel to the grain	kN/mm^2
σ_{para}^{C}	compression strength parallel to the grain	kN/mm^2
τ^F	shear strength	kN/mm^2

The material is assumed to have not failed if the left side of Equation (8.109) is less than 1.0. Equation (8.109) represents an ellipsoid, if plotted in three dimensional space, as a function of shear stress and the two normal stresses. If only a single stress is applied, Equation (8.109) collapses and equals the maximum stress criterion, where maximum stress equals failure stress. Hence, the ellipsoid crosses the three axes at the material strength values. Yet, if more than one stress is applied at once, the maximum stress in any direction may be considerably less *or* substantially higher than material strength in that direction. That is, the criterion may predict strengthening for certain stress combinations such as compressive stress perpendicular and parallel, which means that the extreme points of the ellipsoid do not lie on the coordinate axes. A comprehensive discussion of the Tsai-Wu Criterion for fiber reinforced composite materials (also applicable to wood) can be found in Hyer (1997).

In light of the fact that the stresses computed along the member of a multiple-bolt joint are not constant, and given the desire for the failure criterion to account for crack development and growth, the Tsai-Wu criterion and its application are somewhat modified. First, stress variability along member length and the inclusion of crack development makes it necessary to check for failure in each direction separately by keeping all other stresses constant. To accomplish this, for all but the direction under consideration, the average stress over a given segment between two fasteners, or a fastener and a member end, was computed. The Tsai-Wu criterion is subsequently applied to each length increment of the stress grid (Sec. 8.3.1) varying only the relevant stress per increment. The procedure is repeated for each direction. For example, presuming shear failure is being investigated, the modified criterion may be expressed as

$$C_1 \cdot \overline{\sigma}_{para} + C_2 \cdot \overline{\sigma}_{perp} + C_{11} \cdot \overline{\sigma}^2_{para} + C_{22} \cdot \overline{\sigma}^2_{perp} + C_{66} \cdot \tau(z)^2 - \sqrt{C_{11} \cdot C_{22}} \cdot \overline{\sigma}_{para} \cdot \overline{\sigma}_{perp} = 1.0 \quad (8.115)$$

with

$$\overline{\sigma}_{perp} = \sum_{z=1}^{L} \sigma_{perp}(z) \cdot \frac{z}{L} \quad (8.116)$$

$$\overline{\sigma}_{para} = \sum_{z=1}^{L} \sigma_{para}(z) \cdot \frac{z}{L} \quad (8.117)$$

where L denotes the length of the segment and z is the length increment. All other variables are as previously defined.

Stresses computed by MULTBOLT may exceed material strength of any given direction and stress combination (expressed as Tsai-Wu > or = 1.0). If this is the case, it is assumed that a crack is forming. Consider the shear stress distribution along a member segment between two fasteners depicted in Figure 8.22.

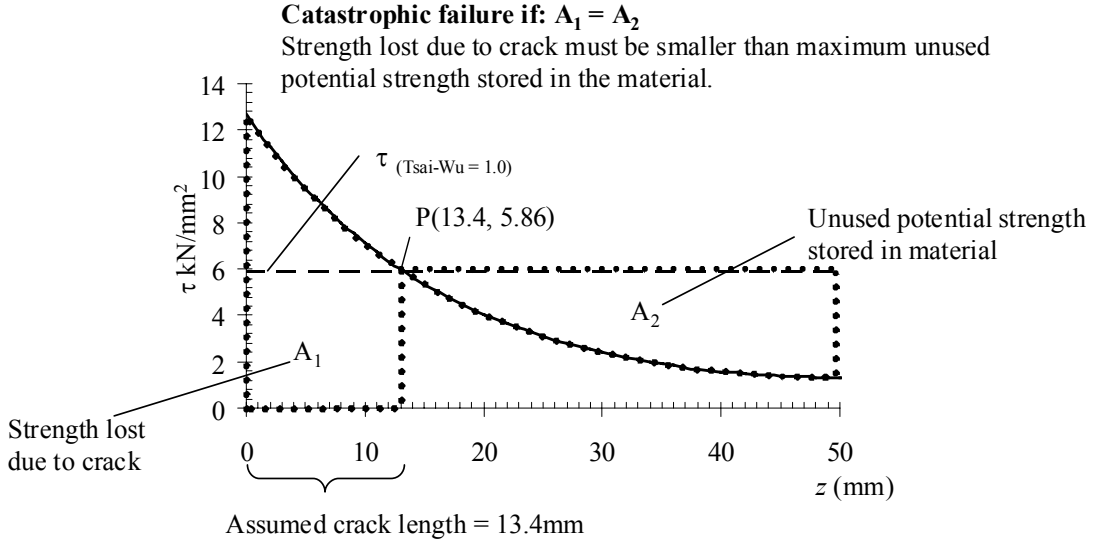

Figure 8.22: Modified failure criterion to include crack development. The dashed line represents the maximum shear strength as predicted by the Tsai-Wu criterion assuming average stresses. The perimeter of area A_1 includes the points 0.0 / 0.0, 0.0 / τ = 12.2, P, z = 13.4 / 0.0, whereas the perimeter of A_2 includes P, z = 50.0 / τ = 1.7, and z = 50.0 / τ = 5.9.

Over a length of 13.4 mm, material strength, as determined by the modified Tsai-Wu criterion, is exceeded and it is consequently assumed that a crack of length 13.4 mm has formed. Thus, the segment where the crack has formed is incapable of resisting shear forces, which means

that the shear force resisted by this segment must be redistributed to the part of the member segment where no crack has formed. Essentially, MULTBOLT checks whether the section without a crack is capable of absorbing the extra force. Thus, if area A_2, which represents the potential strength still stored in the material, is less than area A_1, catastrophic failure occurs. Since stresses are computed at discrete grid points, A_1 may be approximated by numerical integration of the form

$$A_1 = \sum_{j=1}^{nc} \sum_{z=cs_j}^{ce_j} \frac{\tau(z_{i-1}) - \tau(z_i)}{2} \cdot \left(z_{i-1} - z_i\right) \tag{8.118}$$

Note that Equation (8.118) represents the general case. For the stress distributions investigated here, only one crack can be detected per segment. But rather than comparing the two areas to check for failure, a simpler procedure is devised that reaches the same outcome. The total area under the stress distribution curve may be approximated by

$$A_{total} = \sum_{z=0}^{L} \frac{\tau(z_{i-1}) - \tau(z_i)}{2} \cdot \left(z_{i-1} - z_i\right) \tag{8.119}$$

		Units
$\tau(z)$	shear stress at length z	kN/mm^2
z_i	length at grid increment i	mm
i	number of grid increment	
cs	z-position where crack starts (i.e. where material strength is first exceeded)	mm
ce	z-position where crack ends	mm
j	crack number	
nc	total number of cracks detected	
L	length of segment	mm

Furthermore, using the expression

$$cl = \sum_{j=1}^{nc} \sum_{z=cs_j}^{ce_j} \left(z_i - z_{i-1}\right) \Big|_{(Tsai-Wu \geq 1.0)} \tag{8.120}$$

which means that the total detected crack length, cl, is increased by the grid increment at which the Tsai-Wu criterion is greater than or equal to 1.0, and making use of

$$\hat{\tau} = \frac{A_{total}}{cl} \tag{8.121}$$

which yields the equivalent shear stress, $\hat{\tau}$, catastrophic failure occurs if

$$C_1 \cdot \bar{\sigma}_{para} + C_2 \cdot \bar{\sigma}_{perp} + C_{11} \cdot \bar{\sigma}^2_{para} + C_{22} \cdot \bar{\sigma}^2_{perp} + C_{66} \cdot \hat{\tau}^2 - \sqrt{C_{11} \cdot C_{22}} \cdot \bar{\sigma}_{para} \cdot \bar{\sigma}_{perp} \geq 1.0 \quad (8.122)$$

To give an example, if $A_1 = A_2$ in Figure 8.22, then by dividing the total area under the stress distribution curve by *L- cl* = 36.6 mm (50mm – 13.4mm) the stress $\hat{\tau} = 5.86$ is obtained, which, if inserted into Equation (8.122), yields 1.0 and therefore indicates failure. The same procedure is repeated for the two normal stresses using the average shear stress over segment length.

8.5 Failure Model Calibration

The failure model was calibrated with the average test data obtained from ten tests of a single bolt joint yielding in Mode II (refer to Chapter 10). The curves are displayed in Figure 8.23 along with the computed average curve. Mode II was selected because failure is of brittle nature. Only the two nonlinearity parameters Ω_{shear} and Ω_{perp} (for shear stresses and perpendicular to grain stresses, see Figure 8.12) were adjusted to fit the model. It was desired that the model predicts maximum load to occur at approximately the same displacement as stipulated by the average curve of the test data. The two parameters were adjusted by trial and error. Good results were achieved with Ω_{shear} = 2.61 and Ω_{perp} = 0.37 (Figure 8.24). A Ω_{perp} of less than 1.0 signals that failure stresses perpendicular to the grain needed to be amplified by increasing the foundation modulus perpendicular to the grain to produce the desired results. The reason probably lies in the fact that no local peak stresses were included in the stress derivation. By contrast, shear stresses were effectively reduced by dividing the foundation modulus by Ω_{shear} > 1.0, which may be attributed to the assumption that the entire shear force is transferred by the crack planes only.

The calibration relies on the assumption that shear strength and perpendicular-to-grain strength equally affect connection failure. The exact contribution of each strength property is extremely difficult to obtain. Perhaps only detailed finite element analysis of the stresses around a pin-loaded hole in an orthotropic plate beyond elastic loading and valid for slender as well as rigid fasteners could shed some light on the issue. No published records could be found, however, indicating that such an analysis was ever carried out.

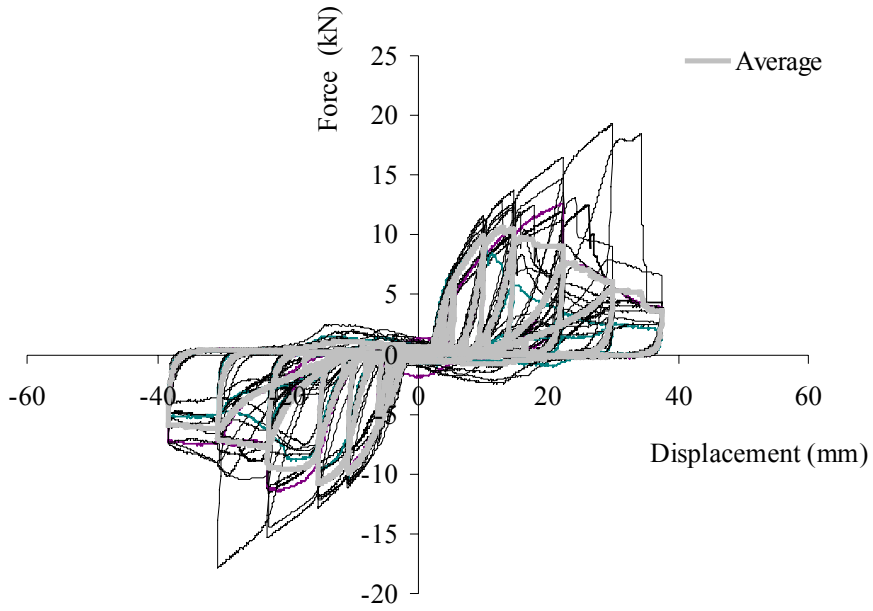

Figure 8.23: Load displacement curves of ten single-bolt specimens yielding in Mode II. The gray curve represents the computed average response.

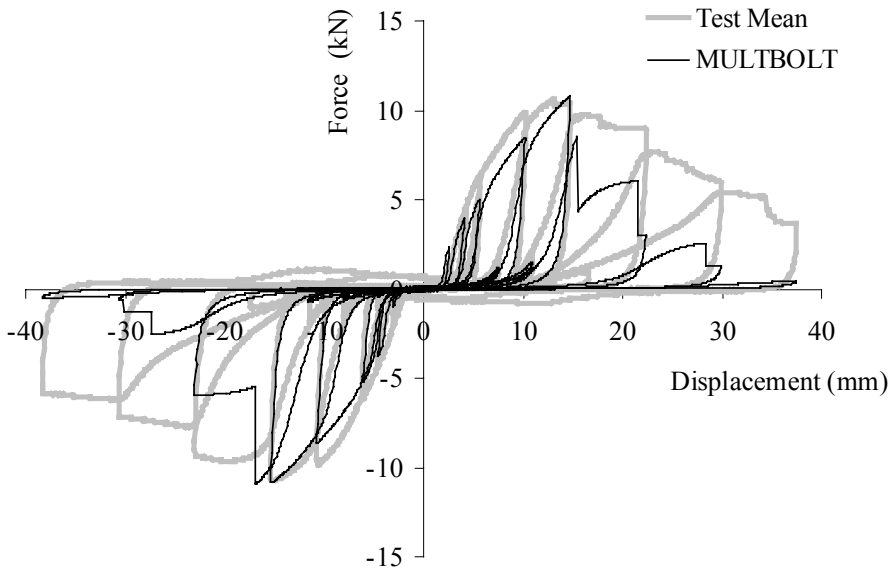

Figure 8.24: Calibration of the failure model using the average curve of data from ten tests on a single bolt joint yielding in Mode II.